

INITIAL POPULATIONS OF BLACK HOLES IN STAR CLUSTERS

KRZYSZTOF BELCZYNSKI^{1,2} ALEKSANDER SADOWSKI³, FREDERIC A. RASIO⁴, TOMASZ BULIK⁵

¹ New Mexico State University, Dept of Astronomy, 1320 Fregner Mall, Las Cruces, NM 88003

² Tombaugh Fellow

³ Astronomical Observatory, Warsaw University, Al. Ujazdowskie 4, 00-478, Warsaw, Poland

⁴ Northwestern University, Dept of Physics and Astronomy, 2145 Sheridan Rd, Evanston, IL 60208

⁵ Nicolaus Copernicus Astronomical Center, Bartycka 18, 00-716 Warszawa, Poland
 kbelczyn@nmsu.edu, oleks@camk.edu.pl, rasio@northwestern.edu, bulik@camk.edu.pl

ABSTRACT

Using an updated population synthesis code we study the formation and evolution of black holes (BHs) in young star clusters following a massive starburst. This study continues and improves on the initial work described by Belczynski, Sadowski & Rasio (2004). In our new calculations we account for the possible ejections of BHs and their progenitors from clusters because of natal kicks imparted by supernovae and recoil following binary disruptions. The results indicate that the properties of both retained BHs in clusters and ejected BHs (forming a field population) depend sensitively on the depth of the cluster potential. In particular, most BHs ejected from binaries are also ejected from clusters with central escape speeds $V_{\text{esc}} \lesssim 100 \text{ km s}^{-1}$. Conversely, most BHs remaining in binaries are retained by clusters with $V_{\text{esc}} \gtrsim 50 \text{ km s}^{-1}$. BHs from single star evolution are also affected significantly: about half of the BHs originating from primordial single stars are ejected from clusters with $V_{\text{esc}} \lesssim 50 \text{ km s}^{-1}$. Our results lay a foundation for theoretical studies of the formation of BH X-ray binaries in and around star clusters, including possible “ultra-luminous” sources, as well as merging BH–BH binaries detectable with future gravitational-wave observatories.

Subject headings: binaries: close — black hole physics — gravitational waves — stars: evolution

1. INTRODUCTION

1.1. Black Holes in Star Clusters

Theoretical arguments and many observations suggest that BHs should form in significant numbers in star clusters. Simple assumptions about the stellar initial mass function (IMF) and stellar evolution indicate that out of N stars formed initially, $\sim 10^{-4} - 10^{-3} N$ should produce BHs as remnants after $\sim 20 \text{ Myr}$. Thus any star cluster containing initially more than $\sim 10^4$ stars should contain at least some BHs; large super star clusters and globular clusters should have formed many hundreds of BHs initially, and even larger systems such as galactic nuclei may contain many thousands to tens of thousands.

Not surprisingly, observations are most sensitive to (and have provided constraints mainly on) the most massive BHs that may be present in the cores of very dense clusters (van der Marel 2004). For example, recent observations and dynamical modeling of the globular clusters M15 and G1 indicate the presence of a central BH with a mass $\sim 10^3 - 10^4 M_{\odot}$ (Gerssen et al. 2002, 2003; Gebhardt et al. 2002, 2005). However, direct N -body simulations by Baumgardt et al. (2003a,b) suggest that the observations of M15 and G1, and, in general, the properties of all *core-collapsed* clusters, could be explained equally well by the presence of many compact remnants (heavy white dwarfs, neutron stars, or $\sim 3 - 15 M_{\odot}$ BHs) near the center without a massive BH (cf. van der Marel 2004; Gebhardt et al. 2005). On the other hand, N -body simulations also suggest that many *non-core-collapsed* clusters (representing about 80% of globular clusters in the Milky Way) could contain central massive BH (Baumgardt et al. 2004, 2005).

In any case, when the correlation between central BH mass and bulge mass in galaxies (e.g., Häring & Rix 2004)

is extrapolated to smaller stellar systems like globular clusters, the inferred BH masses are indeed $\sim 10^3 - 10^4 M_{\odot}$. These are much larger than a canonical $\sim 10 M_{\odot}$ stellar-mass BH (see, however, §3.1.6), but much smaller than the $\sim 10^6 - 10^9 M_{\odot}$ of supermassive BHs. Hence, these objects are often called *intermediate-mass black holes* (IMBHs; see, e.g., Miller & Colbert 2004).

Further observational evidence for IMBHs in dense star clusters comes from many recent *Chandra* and *XMM-Newton* observations of “ultra-luminous” X-ray sources (ULXs), which are often (although not always) clearly associated with young star clusters and whose high X-ray luminosities in many cases suggest a compact object mass of at least $\sim 10^2 M_{\odot}$ (Cropper et al. 2004; Ebisuzaki et al. 2001; Kaaret et al. 2001; Miller et al. 2003). In many cases, however, beamed emission by an accreting stellar-mass BH may provide an alternative explanation (King et al. 2001; King 2004; Zezas & Fabbiano 2002).

One natural path to the formation of a massive object at the center of any young stellar system with a high enough density is through runaway collisions and mergers of massive stars following gravothermal contraction and core collapse (Ebisuzaki et al. 2001; Portegies Zwart & McMillan 2002; Gürkan, Freitag, & Rasio 2004). These runaways occur when massive stars can drive core collapse *before they evolve*. Alternatively, if the most massive stars in the cluster are allowed to evolve and produce supernovae, the gravothermal contraction of the cluster will be reversed by the sudden mass loss, and many stellar-mass BHs will be formed.

The final fate of a cluster with a significant component of stellar-mass BHs remains highly uncertain. This is because realistic dynamical simulations for such clusters (containing a large number of BHs *and* ordinary stars with

a realistic mass spectrum) have yet to be performed. For old and relatively small systems (such as small globular clusters), complete evaporation is likely (with essentially all the stellar-mass BHs ejected from the cluster through three-body and four-body interactions in the dense core). This is expected theoretically on the basis of simple qualitative arguments based on Spitzer’s “mass-segregation instability” applied to BHs (Kulkarni et al. 1993; Sigurdsson & Hernquist 1993; Watters et al. 2000) and has been demonstrated by dynamical simulations (Portegies Zwart & McMillan 2000; O’Leary et al. 2005). However, it has been suggested that, if stellar-mass BHs are formed with a relatively broad mass spectrum (a likely outcome for stars of very low metallicity; see Heger et al. 2003), the most massive BH could resist ejection, even from a cluster with low escape velocity. These more massive BHs could then grow by repeatedly forming binaries (through exchange interactions) with other BHs and merging with their companions (Miller & Hamilton 2002; Gültekin, Miller, & Hamilton 2004). However, as most interactions will probably result in the ejection of one of the lighter BHs, it is unclear whether any object could grow substantially through this mechanism before running out of companions to merge with. A single stellar-mass BH remaining at the center of a globular cluster is very unlikely to become detectable as an X-ray binary (Kalogera, King, & Rasio 2004).

In addition to its obvious relevance to X-ray astronomy, the dynamics of BHs in clusters also plays an important role in the theoretical modeling of gravitational-wave (GW) sources and the development of data analysis and detection strategies for these sources. In particular, the growth of a massive BH by repeated mergers of stellar-mass BHs spiraling into an IMBH at the center of a dense star cluster may provide an important source of low-frequency GWs for LISA, the Laser-Interferometer Space Antenna (Miller 2002; Will 2004). Similarly, dynamical hardening and ejections of binaries from dense clusters of stellar-mass BHs could lead to greatly enhanced rates of BH–BH mergers detectable by LIGO and other ground-based interferometers (Portegies Zwart & McMillan 2000; O’Leary et al. 2005).

A crucial starting point for any detailed study of BHs in clusters is an accurate description of the initial BH population. Here, “initial” means on a timescale short compared to the later dynamical evolution timescale. Indeed most N -body simulations of star cluster dynamics never attempt to model the brief, initial phase of rapid massive star evolution leading to BH formation. The goal of our work here is to provide the most up-to-date and detailed description of these initial BH populations. This means that we must compute the evolution of a large number of massive stars, including a large fraction of binaries, all the way to BH formation, i.e., on a timescale $\sim 10 - 100$ Myr, taking into account a variety of possible cluster environments.

1.2. Previous Work

In a previous study (Belczynski et al. 2004; hereafter Paper I) we studied young populations of BHs formed in a massive starburst, without explicitly taking into account that most stars are formed in clusters. For many repre-

sentative models we computed the numbers of BHs, both single and in various types of binaries, at various ages, as well as the physical properties of different systems (e.g., binary period and BH mass distributions). We also discussed in detail the evolutionary channels responsible for these properties.

In this follow-up study, we consider the possible ejection of these BHs from star clusters with different escape speeds, taking into account the recoil imparted by supernovae (SNe) and binary disruptions. During SNe, mass loss and any asymmetry in the explosion (e.g., in neutrino emission) can impart large extra speeds to newly formed compact objects. If a compact object is formed in a binary system, the binary may either (i) survive the explosion, but its orbital parameters are changed and the system (center-of-mass) speed changes, or (ii) the binary is disrupted and the newly formed compact object and its companion fly apart on separate trajectories. The secondary star in a binary may later undergo a SN explosion as well, provided that it is massive enough. The effects of this second explosion are equally important in determining the final characteristics of compact objects.

In Paper I we included the effects of SNe, both natal kicks and mass loss, on the formation and evolution of BHs (single and in binaries), but we did not keep track of which BHs and binaries would be retained in their parent cluster. Starbursts form most of their stars in dense clusters with a broad range of masses and central potentials (and hence escape speeds; see, e.g., Elmegreen et al. 2002; McCrady et al. 2003; Melo et al. 2005). Smaller clusters of $\sim 10^4 M_\odot$ (open clusters or “young populous clusters,” such as the Arches and Quintuplet clusters in our Galactic center) could have escape speeds as low as $V_{\text{esc}} \lesssim 10 \text{ km s}^{-1}$ while the largest “super star clusters” with much deeper potential wells could have $V_{\text{esc}} \gtrsim 100 \text{ km s}^{-1}$. On the other hand the natal kick velocities could be relatively high, $\sim 100 - 500 \text{ km s}^{-1}$ for low-mass BHs, so that a large fraction of BHs might leave the cluster early in the evolution.

Here we repeat our study of young BH populations taking into account ejections from star clusters. We perform our calculations with a slightly updated version of our population synthesis code **StarTrack** (§2) and we present results for both the retained cluster BH populations and the ejected BHs, which will eventually become part of the field BH population surrounding the surviving clusters. Our models and assumptions are discussed in §2, with particular emphasis on the updates since Paper I. In §3 we present our new results and in §4 we provide a summary and discussion.

2. MODEL DESCRIPTION AND ASSUMPTIONS

2.1. Population Synthesis Code

Our investigation is based on a standard population synthesis method. We use the **StarTrack** code (Belczynski, Kalogera & Bulik 2002, hereafter BKB02), which has been revised and improved significantly over the past few years (Belczynski et al. 2006). Our calculations do not include any treatment of dynamical interactions (collisions) between binaries and single stars or other binaries¹. In particular, the star clusters we consider are assumed to have avoided the ‘runaway collision instability’ that

¹The only exception is that we take into account implicitly the likely mass segregation of massive stars into the cluster core. See §2.3.

can drive rapid collisions and mergers of massive main-sequence stars during an early episode of cluster core collapse (Freitag et al. 2006a,b). Instead, our results can provide highly realistic initial conditions for dynamical simulations of dense star clusters in which the early phase of massive star evolution proceeded ‘normally,’ without significant influence from cluster dynamics.

All stars are evolved based on the metallicity- and wind-mass-loss-dependent models of Hurley, Pols & Tout (2002), with a few improvements described in BKB02. The main code parameters we use correspond to the standard model presented in §2 of BKB02 and are also described in Paper I. Each star, either single or a binary component, is placed initially on the zero-age main sequence (ZAMS) and then evolved through a sequence of distinct phases: main sequence (MS), Hertzsprung Gap (HG), red giant branch (RG), core He burning (CHeB), asymptotic giant branch (AGB); if a star gets stripped of its H-rich envelope, either through wind mass loss or Roche lobe overflow (RLOF) it becomes a naked helium star (He). The nuclear evolution leads ultimately to the formation of a compact object. Depending on the pre-collapse mass and initial composition this may be a white dwarf (WD), a neutron star (NS) or a BH.

The population synthesis code allows us to study the evolution of both single and binary stars. Binary star components are evolved as single stars while no interactions are taking place. We model the following processes, which can alter the binary orbit and subsequent evolution of the components: tidal interactions, magnetic braking, gravitational radiation, and angular momentum changes due to mass loss. Binary components may interact through mass transfer and accretion phases. We take into account various modes of mass transfer: wind accretion and RLOF; conservative and non-conservative; stable or dynamically unstable (leading to common-envelope evolution). The mass transfer rates are calculated from the specific binary configurations and physical properties (masses, evolutionary stages, etc.) of the stars involved. Binary components may lose or gain mass, while the binary orbit may either expand or shrink in response. Moreover, we allow for binary mergers driven by orbital decay. In this study, we evolve binary merger products assuming that they restart on the ZAMS. An exception is made when a BH takes part in the merger, in which case we assume the remnant object to be a BH again. The mass of the merger product is assumed equal to the total parent binary mass for unevolved and compact remnant components; however we assume complete envelope mass loss from any evolved star (HG, RG, CHeB, or evolved He star) involved in a merger.

A few additions and updates to *StarTrack* since Paper I are worth mentioning here (see Belczynski et al. 2006 for more details). System velocities are now tracked for all stars (single and binaries) after SNe (see §2.3). The new magnetic braking law of Ivanova & Taam (2003) has been adopted, although this has minimal impact on our results for BHs. Two new types of WDs have been introduced: hydrogen and ‘hybrid’ (these are possible BH donors in binaries). An improved criterion is adopted for CHeB stars to discriminate between those with convective ($M < 7 M_{\odot}$) and radiative ($M \geq 7 M_{\odot}$) envelopes; this affects the stellar response to mass loss. We have also added a new tidal term for RLOF rate calculations.

Some minor problems in the calculations of Paper I were also identified and are corrected in this study. The evolution of a small fraction of BH RLOF systems with donors at the end of the RG stage was terminated when the donor contracted and detached after entering a CHeB phase. However, the donor may restart RLOF during expansion on the AGB, which is now properly accounted for. Another small fraction of systems, evolving through the rapid RLOF phase with HG donors, were previously classified as mergers and subsequently evolved as single stars (merger products). However, the RLOF at that stage may be dynamically stable and in some cases a binary system may survive and continue its evolution, which is now also properly taken into account. None of these corrections affect the results of Paper I significantly.

2.2. Black Hole Formation

Black holes originate from the most massive stars. The formation time is calculated for each star using the stellar models of Hurley et al. (2000) and Woosley (1986). For intermediate-mass stars the FeNi core collapses and forms a hot proto-NS or a low-mass BH. Part of the envelope falls back onto the central object while the rest is assumed to be ejected in a SN explosion. We use the results of Fryer (1999) and Fryer & Kalogera (2001) to determine how much matter is ejected. In general, for the highest masses ($> 30 M_{\odot}$ for low-metallicity models) total fallback is expected, with no accompanying SN explosion.

Motivated by the large observed velocities of radio pulsars we assume significant asymmetries in SN explosions. Here we adopt the kick velocity distribution of Arzoumanian, Cordes & Chernoff (2002), taking into consideration more recent observations (e.g., White & Van Paradijs 1996; Mirabel & Rodrigues 2003). NSs receive full kicks drawn from the bimodal distribution of Arzoumanian et al. (2002). Many BHs form through partial fall back of material initially expelled in a SN explosion, but then accreted back onto the central BH. For these the kick velocity is lowered proportionally to the mass of accreted material (for details see BKB02). For the most massive stars, the BH forms silently through a direct collapse without accompanying SN explosion, and in this case we assume *no* BH natal kick. The mass loss and kick velocity together determine whether a binary hosting the BH progenitor is disrupted by the SN explosion.

Our calculated initial-to-final mass relation for various metallicities is discussed in detail in Paper I, where it is also demonstrated that (within our BH kick model) for solar metallicity many BHs are formed with lowered kicks through fall back. This occurs for single stars with initial masses in the range $20 - 42 M_{\odot}$ and $50 - 70 M_{\odot}$. For metallicity $Z = 0.001$, BHs receive a kick in the narrower ranges $18 - 25 M_{\odot}$ and $39 - 54 M_{\odot}$, while for $Z = 0.0001$ only BHs formed from stars of $18 - 24 M_{\odot}$ receive kicks, with others forming silently.

2.3. Spatial Velocities

All stars, single and binaries, are assumed to have zero initial velocities. This means we are neglecting their orbital speeds within the cluster. Indeed, for a variety of reasons (e.g., relaxation toward energy equipartition, formation near the cluster center), massive stars (BH progenitors) are expected to have lower velocity dispersions

than the cluster average, itself much lower than the escape speed from the cluster center. We now discuss how to compute the velocities acquired by single stars, binaries, or their disrupted components, following a SN explosion. For disrupted binary components this is, to our knowledge, the first derivation of such results allowing for initially *eccentric* orbits.

Surviving Binaries. For each massive star, the time of the SN event is set by the single star models (taking into account mass variations due to winds and binary interactions). When either component of a binary reaches this stage, we generate a random location in the orbit for the event to take place (note that for eccentric binaries this choice will affect the outcome, since the instantaneous separation and relative velocities are different at different locations along the orbit). The core collapse event is assumed to be instantaneous and the mass of the remnant is calculated as in Paper I. Note that if the remnant is formed through complete fall-back (leading always to direct BH formation), we do not expect a SN explosion (hence no kick and no mass loss) and the orbit remains unchanged (Fryer 1999). When a BH is formed through partial fall-back we treat the event as a SN explosion (see Podsiadlowski et al. 2002).

We calculate the effect of a SN event on binaries in three steps. First, we estimate the mass of the remnant. The rest of the exploding star is immediately lost from the binary (with the specific angular momentum of the exploding component). We assume that the ejecta do not have any effect on the companion. Second, we calculate the compact object velocity, which is the vector sum of the orbital velocity of the pre-collapse star at the random orbital position and the kick velocity. The kick velocity is assumed to be randomly oriented and its magnitude is drawn from our assumed distribution. The kick magnitude is also scaled by the amount of material ejected in the SN explosion,

$$w = (1 - f_{\text{fb}}) * V, \quad (1)$$

where V is the kick magnitude drawn from the assumed distribution, f_{fb} is a fall back parameter (for details see Paper I), and w is the kick magnitude we use in our calculations. For NS remnants with no fall-back ($f_{\text{fb}} = 0$), $w = V$. In our standard model we use a kick magnitude distribution derived by Arzoumanian et al. (2002): a weighted sum of two Gaussians, one with $\sigma = 90 \text{ km s}^{-1}$ (40%) and the second with $\sigma = 500 \text{ km s}^{-1}$ (60%). In the third step, we calculate the total energy (potential and kinetic) of the new orbit for the remnant (new velocity and mass, same relative position) and its companion. If the total energy is positive, then the system is disrupted, and its components will evolve separately. We calculate their subsequent evolution as single stars, and their trajectories are followed (see below). If the total binary energy is negative, the system remains bound after the SN explosion, and we calculate its new parameters (e and A). We also check whether the two components have merged following the SN mass loss and kick, in which case we the evolution of a merger is followed (see § 2.1). These type of mergers are extremely rare and they do not affect our results. Finally, we calculate the post-SN center of mass velocity of the binary.

Disrupted Binaries. The velocities of the stellar components after a system has been disrupted have been calculated by Tauris & Takens (1998) for the case of a circular pre-SN orbit. In this paper we take a more general approach where the pre-SN orbit can have an arbitrary eccentricity. We begin with the coordinate system (I): the center of mass (CM) coordinate system before the SN explosion. At the time of the SN explosion the velocities of the two stars are

$$\vec{v}_1^I = \frac{-M_2 \vec{v}}{M_1 + M_2} \quad (2)$$

$$\vec{v}_2^I = \frac{M_1 \vec{v}}{M_1 + M_2} \quad (3)$$

where \vec{v} is the relative velocity and a superscript I indicates the coordinate system we use. The separation vector between the stars on the orbit at the moment of the SN explosion is $r_0 \vec{n}$. The SN explosion introduces a kick \vec{w} on the newly formed compact star and leads to the ejection of a shell. Thus after the SN explosion star 1 has mass M_{1f} , and its velocity in the pre-SN CM coordinate system (I) is

$$\vec{v}_{1i}^I = \vec{v}_1^I + \vec{w}. \quad (4)$$

The expanding shell (with velocity \vec{v}_{im}) hits the companion. The effects of the impact have been estimated by Wheeler, Lecar and McKee (1975), but it was shown (Kalogera 1996) that they are not large. The velocity of the companion after the expanding shell decouples from the system is

$$\vec{v}_{2i}^I = \vec{v}_2^I + \vec{v}_{im}. \quad (5)$$

In most cases v_{im} is small, and we neglect it in our treatment of the orbits. The direction between the stars remains the same, $\vec{n}^{II} = \vec{n}^I$.

Here we also assume that the shell velocity satisfies $v_{im} \gg r_0/P$ where P is the orbital period of the pre-SN system, so that the shell decouples from the binary instantaneously.

We now introduce a second coordinate system (II): the CM system of the two remaining stars after the explosion. This system moves with the velocity

$$\vec{v}_{CM}^{II} = \frac{M_{1f} \vec{v}_{1i}^I + M_2 \vec{v}_{2i}^I}{M_{1f} + M_2} \quad (6)$$

with respect to system (I). The relative velocity of the two stars (the newly formed compact object and the companion) in this system is

$$\vec{v}^{II} = \vec{v} + \vec{w} - \vec{v}_{im} \quad (7)$$

after shell decoupling. The angular momentum of the two stars is

$$J = \mu r_0 \vec{n}^{II} \times \vec{v}^{II}, \quad (8)$$

where $\vec{n}^{II} = \vec{n}^I$. It is convenient now to introduce the coordinate system (III) in which the angular momentum is aligned with the z -axis. The transformation between (II) and (III) is a simple rotation, which we denote as \mathcal{R} : $v^{III} = \mathcal{R} v^{II}$, $n^{III} = \mathcal{R} n^{II}$. In the coordinate system (III) the two stars move on a hyperbolic orbit described by

$$r = \frac{p}{1 + \epsilon \cos \phi} \quad (9)$$

where

$$p = \frac{J^2}{\alpha\mu} \quad \text{and} \quad \epsilon = \sqrt{1 + \frac{2EJ^2}{\alpha^2\mu}}, \quad (10)$$

$E = \mu(v^{II})^2/2 - \alpha/|r_0|$ is the (positive) energy of the system, $\alpha = GM_{1f}M_2$, and $\mu = M_{1f}M_2/(M_{1f} + M_2)$ is the reduced mass. Using the conservation of energy we find the value of the final relative velocity in (III):

$$|v_f^{III}| = \sqrt{\frac{2E}{\mu}}. \quad (11)$$

It follows from the conservation of angular momentum that the relative velocity \vec{v}_f^{III} at infinity is parallel to the separation vector \vec{n}_f^{III} . The motion is confined to the $x - y$ plane in (III), so what remains now is to find the angle between \vec{n}_f^{III} and \vec{n}_i^{III} . This can easily be found using equation 9. We first find the initial position of the star on the trajectory φ_i (see Fig. 1),

$$\cos \varphi_i = \frac{1}{\epsilon} \left(\frac{p}{r_0 - 1} \right). \quad (12)$$

The sign of the sine of φ_i depends on whether the stars are initially on the ascending or descending branch of the hyperbola. In the ascending branch the scalar product $\vec{v}_i^{III} \vec{r}_0^{III} < 0$, thus

$$\sin \varphi_i = \text{sgn}(\vec{v}_i^{III} \vec{r}_0^{III}) \sqrt{1 - \cos^2 \varphi_i} \quad (13)$$

The final position on the orbit is given by

$$\cos \varphi_f = -\frac{1}{\epsilon}. \quad (14)$$

Finally we see from Fig. 1 that $\sin \varphi_f > 0$.

With these results we can calculate the direction between the stars at $r = \infty$: $n_f^{III} = T(\varphi_f - \varphi_i)n_i^{III}$, where $T(\phi)$ is the matrix of rotation around the z axis. We now have the result that the relative final velocity in the coordinate system (III) is

$$v_f^{III} = \sqrt{\frac{2E}{\mu}} n_f^{III}. \quad (15)$$

We find the velocities of the individual stars in (I) by reversing the path of transformations we followed above,

$$v_{1f}^I = \mathcal{R}^{-1} \left(\frac{-M_2 v_f^{III}}{M_{1f} + M_2} \right) + v_{CM}^{II} \quad (16)$$

$$v_{2f}^I = \mathcal{R}^{-1} \left(\frac{M_{1f} v_f^{III}}{M_{1f} + M_2} \right) + v_{CM}^{II} \quad (17)$$

However, before assuming that these are the final velocities we need to verify that the newly born compact object did not collide with the companion. This may happen if two conditions are satisfied: the stars are initially on the ascending branch of the orbit, and the distance of closest

approach $r_{min} = p/(1 + \epsilon)$ is smaller than the companion radius.

Single Stars. For single stars (either initially single or originating from disrupted binaries), after a SN explosion we simply calculate the remnant mass, add the natal kick velocity to the spatial speed (non-zero for disrupted binaries but zero for primordial single stars) of the object and follow the remnant until the end of the calculation.

2.4. Models

2.4.1. Standard Model

Our standard model (Model A) corresponds to the one in Paper I (also called Model A, with a few minor differences mentioned in §2.1. Here we just reiterate the basic standard model parameters. We evolve both primordial binaries and single stars. Initial stellar masses for single stars and binary primaries are drawn from a three-component, broken power-law IMF with exponent $\alpha_3 = -2.35$ for massive stars, and a flat mass ratio distribution is used to generate secondary masses in binaries. The stars are allowed to reach an initial maximum mass $M_{max} = 150 M_\odot$ (see §2.4.3 for details). Stars are evolved with metallicity $Z = 0.001$ and our adopted standard wind mass loss rates (e.g., Hurley et al. 2000). For the treatment of CE phases we use the standard energy prescription (Webbink 1984) with $\alpha \times \lambda = 1.0$. We adopt $M_{max,NS} = 3 M_\odot$ for the maximum NS mass, and any compact object with mass above this is classified as a BH. As described above we use lowered kicks for fall-back BHs and no kicks for direct BHs.

2.4.2. Alternative Models

We also performed a set of calculations for a number of different models in order to test the influence of our most important assumptions and model parameters on BH formation. Each alternative model differs from our standard reference model in the value of one particular parameter or with a change in one particular assumption. All models are described in Table 1. Note that we added one model not present in Paper I: in Model J, we use an alternative prescription for CE phases based on angular momentum balance with parameter $\gamma = 1.5$ (see Belczynski, Bulik & Ruiter 2005 and references therein), as opposed to the standard energy balance used in all other models. It has been claimed that this alternative CE prescription leads to better agreement with the observed properties of WD binaries in the solar neighborhood (Nelemans & Tout 2005). We wish to test whether this new CE prescription has any effect on our predictions for young BH populations. For some of alternative models (Models B, D, I and J) the evolution of single stars is not affected and we use the single star population from the standard model. However, we calculate the separate single star populations for models in which the single star evolution is changed with a given parameter (Models C1, C2, E, F, G1, G2 and H).

2.4.3. Initial Conditions and Mass Calibration

In addition to a brief description of each model, Table 1 also gives the total initial mass in single and binary stars. All stars are assumed to form in an instantaneous burst of star formation. Single stars and binary components are assumed to form from the hydrogen burning limit ($0.08 M_\odot$) up to the maximum mass M_{max} characterizing a

given system. Masses of single stars and binary primaries (more massive components) are drawn from the three-component, power-law IMF of Kroupa, Tout, & Gilmore (1993) (see also Kroupa & Weidner 2003) with slope $\alpha_1 = -1.3$ within the initial mass range $0.08 - 0.5 M_\odot$, $\alpha_2 = -2.2$ for stars within $0.5 - 1.0 M_\odot$, and $\alpha_3 = -2.35$ within $1.0 M_\odot - M_{\max}$. The binary secondary masses are generated from an assumed flat mass ratio distribution ($q = M_a/M_b$; M_a , M_b denoting the mass of the primary and secondary, respectively). The mass ratio is drawn from the interval q_{\min} to 1, where $q_{\min} = 0.08 M_\odot/M_a$, ensuring that the mass of the secondary does not fall below the hydrogen burning limit. The only exception is model B, in which both the primary and the secondary masses are sampled independently from the assumed IMF (i.e., the component masses are not correlated). This IMF is easily integrated to find the total mass contained in single and binary stars for any adopted $\alpha_1, \alpha_2, \alpha_3$ values. The particular choice of low-mass slope of the IMF (α_1, α_2) does not change our results, since low-mass stars do not contribute to the BH populations. However, as most of the initial stellar mass is contained in low-mass stars, a small change in the IMF slope at the low-mass end can significantly change the mass normalization.

In our simulations, we do not evolve all the single stars and binaries described above since the low-mass stars cannot form BHs. Out of the total population described above we evolve only the single stars with masses higher than $4 M_\odot$ and the binaries with primaries more massive than $4 M_\odot$ (no constraint is placed on the mass of the secondary, except that it must be above $0.08 M_\odot$). All models were calculated with 10^6 massive primordial binaries. We also evolved 2×10^5 massive single stars but then scaled up our results to represent 10^6 single stars. The mass evolved in single stars and binaries was then calculated and, by extrapolation of the IMF (down to hydrogen burning limit), the total initial cluster mass was determined for each model simulation.

In the discussion of our results we assume an initial (primordial) binary fraction of $f_{\text{bin}} = 50\%$, unless stated otherwise (i.e., tables and figures usually assume equal numbers of single stars and binaries initially, with $2/3$ of stars in binaries). However, our results can easily be generalized to other primordial binary fractions f_{bin} by simply weighing differently the numbers obtained for single stars and for binaries.

Our assumed distribution of initial binary separations follows Abt (1983). Specifically, we take a flat distribution in $\log a$, so that the probability density $\Gamma(a) \propto \frac{1}{a}$. This is applied between a minimum value, such that the primary's initial radius (on the zero-age main sequence) is half the radius of its Roche lobe, and a maximum value of $10^5 R_\odot$. We also adopt a standard thermal eccentricity distribution for initial binaries, $\Xi(e) = 2e$, in the range $e = 0 - 1$ (e.g., Heggie 1975; Duquennoy & Mayor 1991).

2.4.4. Cluster Properties

The only cluster parameter that enters directly in our simulations is the escape speed V_{esc} from the cluster core. All single and binary BHs are assumed immediately ejected from the cluster if they acquire a speed exceed-

ing V_{esc} . We do not take into account ejections from the cluster halo (where the escape speed would be lower) as all BHs and their progenitors are expected to be concentrated near the cluster center.

In Tables 2, 3, 4, 5 we present results of simulations for our standard model corresponding to four different values of the escape speed: $V_{\text{esc}} = 10, 50, 100, 300 \text{ km s}^{-1}$. For any assumed cluster model the escape speed can be related to the total mass M_{cl} and half-mass radius R_{h} :

$$V_{\text{esc}} = f_{\text{cls}} \left(\frac{M_{\text{cl}}}{10^6 M_\odot} \right)^{1/2} \left(\frac{R_{\text{h}}}{1 \text{ pc}} \right)^{-1/2}. \quad (18)$$

For example, for a simple Plummer sphere we have $f_{\text{cls}} = 106 \text{ km s}^{-1}$, while for King models with dimensionless central potentials $W_0 = 3, 5, 7, 9$ and 11 , the values are $f_{\text{cls}} = 105.2, 108.5, 119.3, 157.7$, and 184.0 km s^{-1} , respectively. For our four considered values of the escape speed, $V_{\text{esc}} = 10, 50, 100$, and 300 km s^{-1} , in a $W_0 = 3$ King model with $R_{\text{h}} = 1 \text{ pc}$ (typical for a variety of star clusters), the corresponding cluster masses are $M_{\text{cl}} = 0.009, 0.226, 0.904$, and $8.132 \times 10^6 M_\odot$, respectively.

In each table we present the properties of BH populations at five different cluster ages: 8.7, 11.0, 15.8, 41.7 and 103.8 Myr. These correspond to MS turnoff masses of 25, 20, 15, 8 and $5 M_\odot$, respectively. The tables include information on both the BHs retained in the clusters (with velocities $< V_{\text{esc}}$) and those ejected from clusters.

3. RESULTS

3.1. Standard Reference Model

3.1.1. Black Hole Spatial Velocities

In Figure 2 we show distributions of spatial velocities for *all* single and binary BHs shortly after the initial starburst (at 8.7 Myr). The distribution shows a rather broad peak around $\sim 30 - 300 \text{ km s}^{-1}$, but also includes a large fraction ($\sim 2/3$) of BHs formed with no kick. The peak originates from a mixture of low-velocity binary BHs and high-velocity single BHs. The no-kick single and binary BHs originate from the most massive stars, which have formed BHs silently and without a kick. All the no-kick systems (with zero velocity assumed) were placed on the extreme left side of all distributions in Figure 2 to show their contribution in relation to other non-zero velocity systems (the bin area is chosen so as to represent their actual number, although the placement of the bin along the velocity axis is arbitrary). Binary stars hosting BHs survive only if the natal kicks they received were relatively small, since high-magnitude kicks tend to disrupt the systems. We see (middle panel of Fig. 2) that most BH binaries have spatial velocities around 50 km s^{-1} , which originate from the low-velocity side of the bimodal Arzoumanian et al. (2002) distribution. Single BHs originating from single stars follow closely the bimodal distribution of natal kicks, but the final BH velocities are slightly lower because of fall-back and direct BH formation (see §2.3). The low- and high-velocity single BHs have speeds around 50 km s^{-1} and 250 km s^{-1} , respectively. Single BHs originating from binary disruptions gain high speeds ($\sim 100 - 400 \text{ km s}^{-1}$), since binaries

¹Statistics is much better for single stars than binaries; and even with only 2×10^5 single stars we obtain usually thousands, and minimum several hundred, BHs. For example see Tables 2-5

are disrupted when a high-magnitude kick occurs. Finally, the single BHs formed through binary mergers have the lowest (nonzero) velocities ($\sim 10 - 100 \text{ km s}^{-1}$), since they are the most massive BHs and therefore most affected by fall-back.

In Figure 3 we show the velocity distributions at a later time (103.8 Myr) when essentially all BHs have formed, and no more SNe explosions are expected, so the velocity distribution is no longer evolving (the MS turnoff mass for that time is down to $5 M_{\odot}$). The velocities have now shifted to somewhat higher values (with a single peak at $\simeq 200 \text{ km s}^{-1}$ for non-zero velocity BHs), while the relative contribution of no-kick systems drops to around 1/3. At this later time the population is more dominated by single BHs. Most of the non-zero velocity single BHs come from binary disruptions (see middle panel of Fig. 3) and therefore they have received larger kicks, shifting the overall distribution toward slightly higher velocities. Also, at later times, lower-mass BH progenitors go through SN explosions, and they receive on average larger kicks (since for lower masses there is less fall back).

We note that most of the non-zero-velocity BHs gain speeds of $50 - 200 \text{ km s}^{-1}$ in SNe explosions. Depending on the properties of a given cluster they may be ejected or retained, and will either populate the field or undergo subsequent dynamical evolution in the cluster. We now discuss separately the properties of the retained and ejected BH populations.

3.1.2. *Properties of Retained (Cluster) BH Populations*

Retained BHs in clusters could be found either in binaries or as single objects. Binary BHs are found with different types of companion stars, while single BHs may have formed through various channels, which we also list in Tables 2 – 5. Shortly after the starburst the most frequent BH companions are massive MS stars, but, as the population evolves, these massive MS companions finish their lives and form additional BHs. Double BH–BH systems begin to dominate the binary BH population after about 15 Myr. At later times less massive stars evolve off the MS and start contributing to the sub-population of BHs with evolved companions (CHeB stars being the dominant companion type, with a relatively long lifetime in that phase) or other remnants as companions (WDs and NSs). Once the majority of stars massive enough to make BHs end their lives (around $10 - 15 \text{ Myr}$) we observe a general decrease in the total number of BHs in binaries. The number of BHs in binaries is depleted through the disruptive effects of SNe and binary mergers (e.g., during CE phases). Both processes enhance the single BH population. This single population is dominated by the BHs formed from primordial single stars (assuming $f_{\text{bin}} = 50\%$). The formation along this single star channel stops early on when all single massive stars have finished evolution and formed BHs (at $\simeq 10 - 15 \text{ Myr}$). In contrast, the contribution of single BHs from binary disruptions and mergers is increasing with time, but eventually it also saturates (at $\simeq 50 - 100 \text{ Myr}$), since there are fewer potential BH progenitor binaries as the massive stars die off. In general, the single BHs are much more numerous in young cluster environments than binary BHs. At early times ($\simeq 10 \text{ Myr}$) they dominate by a factor 2–4, but later the ratio of single to binary BHs increases to almost 10 (after $\sim 100 \text{ Myr}$),

as many binaries merge or are disrupted (adding to the single population).

3.1.3. *Properties of Ejected (Field) BH Populations*

Tables 2 – 5 show also the properties of BHs ejected from their parent clusters, assuming different escape speeds. Significant fractions ($\gtrsim 0.4$) of single and binary BHs are likely to be ejected from any cluster with escape speed $V_{\text{esc}} \lesssim 100 \text{ km s}^{-1}$. In general, single BHs are more prone to ejection since they gain larger speeds in SNe explosions (compared to heavier binaries). Early on the number of ejected BHs increases with time as new BHs of lower mass (and hence receiving larger kicks) are being formed. At later times (after $\simeq 15 \text{ Myr}$), the number of fast BHs remains basically unchanged. Ejected binaries consist mostly of BH–MS and BH–BH pairs in comparable numbers. Rare BH–NS binaries are ejected more easily than other types since they experience two kicks. Single ejected BHs consist mostly of BHs originating from single stars which have received large kicks and from the components of a disrupted binary (the involved kicks were rather large to allow for disruption).

3.1.4. *Dependence on Cluster Escape Velocity and Initial Binary Fraction*

In Table 6 we list fractions of retained BHs at 103.8 Myr after the starburst. The results are presented for initial cluster binary fractions of $f_{\text{bin}} = 0, 50, 100\%$, and can be linearly interpolated for the desired f_{bin} . For our standard model the results are shown for the four considered escape velocities. For an initial cluster binary fraction $f_{\text{bin}} = 50\%$ we find that the retained fraction can vary from ~ 0.4 for low escape velocities ($V_{\text{esc}} = 10 \text{ km s}^{-1}$) to ~ 0.9 for high velocities ($V_{\text{esc}} = 300 \text{ km s}^{-1}$). For escape velocities typical of globular clusters or super star clusters ($V_{\text{esc}} \sim 50 \text{ km s}^{-1}$), retained and ejected fractions are about equal. The retained fractions for various types of systems are plotted as a function of V_{esc} in Figure 4. All curves are normalized to total number of BHs, both single and binaries.

Results are listed in Table 6 for different binary fractions. In particular, these can be used to study the limiting cases of pure binary populations ($f_{\text{bin}} = 100\%$) and pure single star populations ($f_{\text{bin}} = 0\%$). Note that even an initial population with all massive stars in binaries will form many single BHs through binary disruptions and binary mergers. We also note the decrease of the retained fraction with increasing initial binary fraction. Clusters containing more binaries tend to lose relatively more BHs through binary disruptions in SNe compared to single star populations.

3.1.5. *Orbital Periods of Black Hole Binaries*

Figure 5 presents the period distribution of BH binaries for our standard model (for the characteristic escape velocity $V_{\text{esc}} = 50 \text{ km s}^{-1}$). We show separately populations retained and ejected from a cluster. The distributions for different values of the escape velocity are similar.

In Paper I we obtained a double-peaked period distribution for BHs in field populations: tighter binaries were found around $P_{\text{orb}} \sim 10 \text{ d}$ while wider systems peaked around $P_{\text{orb}} \sim 10^5 \text{ d}$. The shape of this distribution comes

from the property that tighter BH progenitor systems experienced at least one RLOF/CE episode leading to orbital decay, while wider systems never interacted and stayed close to their initial periods. The two peaks are clearly separated with a demarcation period $P_s \sim 10^3$ d.

It is easily seen here that slow and fast BH populations add up to the original double-peaked distribution of Paper I. Only the shortest-period and hence most tightly bound systems ($P_{\text{orb}} < P_s$) survive SN explosions and they form a population of fast, short-period BH binaries (see bottom panel of Fig. 5). In contrast, systems retained in clusters have again a double-peaked orbital period distribution. The slowest systems have rather large periods ($P_{\text{orb}} \sim 10^5$ d) and they will likely get disrupted through dynamical interactions in the dense cluster core. The short-period cluster binaries ($P_{\text{orb}} \sim 10 - 100$ d) are much less numerous, since most of the short-period systems gained high post-SN velocities and contributed to the ejected population. Compared to Paper I we note that the inclusion of ejections further depletes the cluster *hard* binary BH population. Only about 1/3 of systems are found with periods below P_s , half of which are retained within a cluster with $V_{\text{esc}} = 50 \text{ km s}^{-1}$. For a cluster with $V_{\text{esc}} = 100 \text{ km s}^{-1}$ about 80% of the short-period systems are retained.

3.1.6. Black Hole Masses

Black hole mass distributions are presented in Figures 6, 7 for $V_{\text{esc}} = 50 \text{ km s}^{-1}$. With few exceptions the models for different escape velocity values are very similar. The retained and ejected populations are shown in separate panels.

The retained populations of BHs shown in the top panel of Figure 6 have a characteristic triple-peaked mass distribution: a first peak at $M_{\text{BH}} \sim 6 - 8 M_{\odot}$, a second one at $M_{\text{BH}} \sim 10 - 16 M_{\odot}$, and third at $M_{\text{BH}} \sim 22 - 26 M_{\odot}$; beyond this it steeply falls off with increasing mass.

The shape of the distribution is determined by the combination of IMF and initial-to-final mass relation for single BHs (presented and discussed in detail in Paper I): the most massive stars ($\geq 50 M_{\odot}$) form BHs with masses in the range $\sim 10 - 16 M_{\odot}$; stars within an initial mass range $25 - 35 M_{\odot}$ form BHs of mass $\sim 25 M_{\odot}$; stars of initially $40 - 50 M_{\odot}$ tend to form $7 M_{\odot}$ BHs. Both single and binary BHs contribute significantly to the second and third peaks. However, only single stars are responsible for a first narrow peak corresponding to a pile up of BHs in the initial-to-final mass relation around $6 - 8 M_{\odot}$. This characteristic feature is a result of a very sharp transition in single star evolution, from H-rich to naked helium stars, which is caused by wind mass loss and the more effective envelope removal for single stars above a certain initial mass. In binary stars, removal of the envelope can happen not only through stellar winds but also through RLOF, and so it is allowed for the entire mass range and the first peak is washed out.

The ejected populations, shown in the bottom panel of Figure 6, are dominated by single BHs (due to their high average speeds) with masses $\sim 3 - 30 M_{\odot}$. The distributions have one sharp peak at $M_{\text{BH}} \sim 6 - 8 M_{\odot}$, corresponding to the first low-mass peak in the distribution for retained populations. The high-mass BHs are very rare in the ejected populations since the kick magnitudes decrease

with increasing BH mass (because of significant fall-back or direct BH formation at the high-mass end).

BHs in binary systems reach a maximum mass of about $30 M_{\odot}$ for both cluster and ejected populations. Most single BHs have masses below $30 M_{\odot}$. However, the tail of the single BH mass distribution extends to $\sim 50 M_{\odot}$ for ejected populations and to about $80 M_{\odot}$ for cluster populations. This is shown in Figure 7 (note a change of vertical scale as compared to Figure 6). The highest-mass BHs are always retained in the clusters and they are formed through binary mergers. These mergers are the result of early CE evolution of massive binaries. The most common merger types are MS–MS, HG–MS and BH–HG mergers. During mergers involving HG stars we assume that the envelope of the HG star is lost, while the BH/MS star and the compact core of the HG star merge to form a new, more massive object. The merger product is then evolved and it may eventually form a single BH.

Even with significant mass loss through stellar winds and during the merger process, a small fraction of BHs reach very high masses, up to about $80 M_{\odot}$. With a less conservative assumption, allowing some fraction of the HG star envelope to be accreted onto the companion in a merger, the maximum BH mass could then reach even higher values $\gtrsim 100 M_{\odot}$. In Figure 8 we show the results of a calculation with the merger product’s mass always assumed equal to the total binary mass.

Although the amount of mass loss in a merger is rather uncertain, the two models above (with and without mass loss) indicate that binary star evolution could lead to the formation of single $\sim 100 M_{\odot}$ BHs. These most massive BHs form very early in the evolution of a cluster (first $\sim 5 - 10$ Myr) since they originate from the most massive and rapidly evolving stars. These BHs are retained in clusters (direct/silent BH formation with no associated natal kick) and they may act as potential seeds for building up intermediate-mass BHs through dynamical interactions during the subsequent cluster evolution (Miller & Hamilton 2002; O’Leary et al. 2005).

3.2. Parameter Study

3.2.1. Black Hole Spatial Velocities

For most alternative models the velocity distributions are similar to those found in the reference model (see Fig. 2 and 3). These distributions are generally characterized by the same wide, high-velocity peak (tens to hundreds of km s^{-1}) and a rather large population of zero-kick BHs. In particular, for models B, F, G2, J and H, the distributions are almost identical to those of the reference model at all times. For models D, G1, and I the distributions show slight differences. With lowered CE efficiency (model D) it is found that there are fewer fast binary BHs, and most surviving binaries do not gain higher velocities at early times. Basically, many tight binaries that survived SN explosions in the reference model have now merged in a first CE phase, even before the first SN explosion occurred. In model G1, in which we consider only primordial stars up to $M_{\text{max}} = 50 M_{\odot}$, the population of massive BHs formed through direct collapse (with no kick) is significantly reduced. This results in a velocity distribution similar to that of the reference model for non-zero velocity systems, but with a much lower number of zero-kick BHs.

The model I distribution is slightly different, especially at early times when most BHs form with no kick, since in this model we consider only the most massive BHs formed mainly through direct collapse.

A few models show more significant differences. Different metallicities lead to changes in BH velocities, especially at early times. For very low metallicity (model C1) almost all BHs are formed with no kick, while for high, solar-like metallicity (model C2) most BHs have non-zero velocities in a wide range ($\sim 10 - 1000 \text{ km s}^{-1}$). Metallicity strongly affects the wind mass loss rates, which are most important for the evolution of the most massive stars (i.e., at early times). In particular, for low- Z values, the wind mass loss rates are smaller (hence more high-mass pre-SN stars and direct collapses), while for high Z the winds are very effective in removing mass from BH progenitors (hence smaller mass pre-SN stars, and more fall-back BH formation). The most significant difference is found in model E, where we allow for full BH kicks. All BHs are formed with rather high ($\geq 100 \text{ km s}^{-1}$) velocities. The distribution, shown in Figures 15 and 16, is double-peaked both for early and late times. The single stars dominate the population, forming the low- ($\sim 100 \text{ km s}^{-1}$) and high-velocity component ($\sim 500 \text{ km s}^{-1}$), a direct result of the adopted bimodal natal kick velocity distribution. Binary stars are found at lower velocities ($\sim 100 \text{ km s}^{-1}$) but they are only a minor contributor to the overall BH population since most of them are now disrupted at the first SN explosion.

3.2.2. *Properties of Retained (Cluster) BH Populations*

In Table 7 we present the properties of cluster BH populations 11 Myr after the starburst. Results for the various models may be easily compared with our reference model.

Binary BHs for different model assumptions are still in general dominated by BH-MS and BH-BH binaries. These systems appear in comparable numbers in most models. Only for models B and E do we find a smaller contribution of BH-BH binaries ($\sim 5\%$ and almost zero for models E and B, respectively). In model B the independent choice of masses produces systems with extreme mass ratios, so that massive primordial binaries with two BH progenitors are very rare. Obviously for model E, in which the two BHs receive full kicks, the BH-BH binary formation is strongly suppressed by binary disruptions. The highest number of binaries containing BHs is found in our model with the lowest tested metallicity (C1). For low metallicities BHs form preferentially with high masses (low wind mass loss rates) through direct collapse with no kick. In contrast model E, assuming full BH kicks, results in the lowest number of BH binaries. Many models (D, G2, H, I, J) result in very similar contents to our reference model. It is worth noting in particular that the CE treatment (either lowered efficiency in model D, or different prescription in model J) does not appear to play a significant role in determining cluster initial binary BH populations.

For all models the single BHs dominate the population even at very early times (as early as 11 Myr). Single BHs originate predominantly from primordial single stars, with smaller contributions from disrupted binaries and binary mergers. The basic general trends seen in our reference model are preserved in other models. Also most models (B, C1, D, G2, H, I, J) form similar numbers of single BHs as our reference model. It is found, as in the binary pop-

ulations, that the highest number of single BHs is seen in our model with lowest metallicity (C1), while the model with full BH kicks (E) generates the lowest number of single BHs retained in a cluster.

At 103.5 Myr (see Table 8), when no more BHs are being formed, single BHs strongly dominate (by about an order of magnitude) over binary BHs. Single BHs still originate mostly from primordial single stars, but there is an increased contribution from binary mergers and disruptions. The binary population remains dominated by BH-BH and BH-MS systems in most models, but with an increased contribution from other evolved systems (BH-WD and BH-NS) compared to earlier times. Note that only in model E does the number of systems other than BH-BH and BH-MS end up dominating the binary population.

3.2.3. *Properties of Ejected (Field) BH Populations*

In Tables 7 and 8 we also characterize the populations of ejected (field) BHs for various models. Results for both times are comparable for binary BHs, but with significantly more single BHs being ejected at later times.

The BH-MS and BH-BH binaries, which dominate the total populations, are also found to be most effectively ejected from clusters. However, BH-NS systems, receiving two natal kicks, are also found to be easily ejected. Indeed, in many models (C1, C2, E, F, G1, G2, H, J), they constitute a significant fraction of ejected systems. Contrary to our intuitive expectation, evolution with the full BH kicks (model E) does not generate a particularly large population of fast BH binaries. In fact, the ejected population is smaller than in the reference model. Higher kicks are much more effective in binary disruption than in binary ejection.

The numbers of fast single BHs are comparable in most models (A, B, D, G1, G2, H, J), with the ejected populations usually consisting equally of BHs coming from binary disruptions and primordial single stars, with a smaller contribution from merger BHs. For models with massive BHs (C1 and I) which receive small kicks there are fewer single BHs in the ejected population (by a factor ~ 2). On the other hand, for the model with full BH kicks (E), the ejected single BH population is larger (by a factor of ~ 3) compared to the reference model.

3.2.4. *Dependence on Cluster Escape Velocity and Initial Binary Fraction*

Retained fractions for different evolutionary models follow in general the same trends as in our reference model, i.e., retained fractions decrease with increasing initial binary fraction. The exception to that trend is for models with full BH kicks (E), increased metallicity (C2) or uncorrelated binary component masses (B). Also, independent of the escape velocity, it is found that at least $\sim 40\%$ of BHs are retained simply because of no-kick BHs (for an initial binary fraction of 50%), with the obvious exception of the model with full BH kicks (E). In particular, for models C1, D, F, G1, G2, H, I, and J, the dependence of the retained fraction on V_{esc} is very similar to that seen in the reference model (see Fig. 4).

In model B, the secondary mass is on average very small compared to the BH mass (due to our choice of initial conditions for this model). Therefore, BHs in binary systems

gain similar velocities (almost unaffected by their companions) as single BHs, and this leads to almost constant fraction of retained systems (~ 0.64) independent of the initial binarity of the cluster. In models C2 and E the fraction of retained systems may be as small as 0.4 and 0, respectively. In our model with high metallicity (C2), as discussed above (§ 3.2.1), high wind mass loss rates lead to higher BH kicks and hence smaller retained fractions. The most dramatic change is observed for model E, with full BH kicks. The retained fractions for this model are shown in Figure 17. Here, we also normalize all curves to the total number of BHs (single and in binaries). The retained fraction increases from 0 to ~ 0.9 , approximately proportional to the escape velocity, with no apparent flattening up to $V_{\text{esc}} \sim 1000 \text{ km s}^{-1}$ as a result of the high speeds BHs receive at formation. The total retained fraction does not reach unity, since there is still a small number of BHs with velocities over 1000 km s^{-1} . Larger BH kicks (switching from standard lowered kicks to full kicks) decrease the retained fraction from 0.6 to 0.2 for $V_{\text{esc}} \simeq 50 \text{ km s}^{-1}$ and $f_{\text{bin}} 50\%$.

A summary of retained and ejected fractions for different initial cluster binary fractions is presented in Table 6 for $V_{\text{esc}} = 50 \text{ km s}^{-1}$. In particular, we show results for pure single star populations ($f_{\text{bin}} = 0\%$) and for all binaries ($f_{\text{bin}} = 100\%$). Note that single star populations will obviously form only single BHs, while the binary-dominated clusters will form both BH binaries and single BHs (through disruptions and mergers)².

For the standard $f_{\text{bin}} = 50\%$ it is found that the retained fraction of BHs varies from 0.4 – 0.7 across almost all models. The only exception is model E with full BH kicks for which the retained fraction is only 0.2. For more realistic and higher initial cluster binary fractions ($f_{\text{bin}} = 75 - 100\%$; see Ivanova et al. 2005) the retained BH fraction is found in an even narrower range 0.4 – 0.6 (again with the exception of model E). Therefore, despite the number of model uncertainties, the initial BH cluster populations, as far as the numbers are concerned, are well constrained theoretically. The issue of BH kicks is not resolved yet, but both observational work (e.g., Mirabel & Rodrigues 2003) and theoretical studies (e.g., Willems et al. 2005) are in progress.

3.2.5. Orbital Periods of Black Hole Binaries

In Figures 9 and 10 we show the dependence of the period distributions of BH binaries on model assumptions. In general, the period distribution remains bimodal in most of the models (B, C1, C2, D, F, G1, G2, H) for retained BH binaries, while only short-period binaries tend to be ejected from clusters, as explained in § 3.1.5. Most of the retained binaries are formed with rather large orbital periods (with the exception of model E, see below) and they will be prone to dynamical disruption in dense cluster environments.

The major deviations from the reference model are found for model E, with full BH kicks. The retained population is rather small as compared to the other models and consists mostly of short-period binaries, since all of the wide BH systems were disrupted by SN natal kicks. The majority of short-period binaries which survived gained

significant velocities ($\geq 50 \text{ km s}^{-1}$; see Fig. 16) and the ejected population is the most numerous in this model.

In several other models we find smaller variations from the reference period distribution. Models with different CE efficiency and treatment (D and J), in which most close binaries merge, have very small numbers of short-period binaries. Also, the model in which we consider only the most massive BHs (descendants of wide primordial binaries) is characterized by a smaller short-period binary population.

3.2.6. Black Hole Masses

In Figures 11 and 12 we present the BH mass distributions from all the models in our study, for both single and binary BH populations.

The shape of the distribution for the retained and ejected BH populations is not greatly affected by different choices of parameter values, with the exception of metallicity and BH kicks (see Fig. 11). This is easily understood, as the highest-mass BHs are formed only at low metallicity (Models C1 and A) and the lightest BHs are formed at high metallicity (Model C2). For full BH kicks (model E) the majority of BHs gain high speeds, and the mass distribution for the ejected population is similar to the combination of ejected and retained populations in the reference model.

Most of the BHs do not exceed $\sim 25 M_{\odot}$. However, a small fraction of single BHs in many models reach very high masses around $80 M_{\odot}$. Figures 13 and 14 show the mass distributions of single BH subpopulations. In all the models with high-mass BHs the most massive BHs are formed through binary mergers. In all the calculations presented here we have assumed mass loss during the merger process if an evolved star was involved (as discussed in § 3.1.6). The highest maximum BH masses are found in the lowest metallicity environments (models A and C1), in larger systems (with high M_{max} , model G2), and for binaries formed with full BH kicks (model E), quite independent of other evolutionary parameters. We find $\sim 10 - 100$ BHs with masses over $60 M_{\odot}$ in models C1, C2, E, G2 and J (and fewer in other models), for a total starburst mass of $\sim 10^8 M_{\odot}$ (see Table 1). The highest mass BHs are retained in clusters with the exception of the model incorporating full BH kicks, in which they are found both with high and low speeds. Only in a few models, with uncorrelated initial binary component masses (B), low CE efficiency (D), or low M_{max} (G1), does the maximum BH mass stay below $\sim 60 M_{\odot}$. And in particular, in the model B, the maximum BH mass stay below $\sim 30 M_{\odot}$. This is due to the fact, that in this model BHs are accompanied by relatively low mass companions and therefore there is no mass reservoir to increase substantially initial (formation) BH mass.

4. SUMMARY AND DISCUSSION

Using the population synthesis code **StarTrack** we have studied the formation of single and binary BHs in young star clusters. Our study continues and improves on the initial work described in Paper I by taking explicitly into account the likely ejections of BHs and their progenitors from

²The number of single BHs formed out of binary systems may be inferred by comparing the numbers of binary BHs with the single BHs listed under “binary disruption” and “binary mergers” in Tables 2–5, 7 and 8

star clusters because of natal kicks imparted by SNe or recoil following binary disruptions. The results indicate that the properties of both retained BHs in clusters and ejected BHs (forming a field population) depend sensitively on the depth of the cluster potential. For example we find that most BHs ejected from binaries are also ejected from clusters with central escape speeds $V_{\text{esc}} \lesssim 100 \text{ km s}^{-1}$, while most BHs remaining in binaries are retained by clusters with $V_{\text{esc}} \gtrsim 50 \text{ km s}^{-1}$. Also, approximately half of the single BHs originating from the primordial single star population are ejected from clusters with $V_{\text{esc}} \lesssim 50 \text{ km s}^{-1}$. The overall BH retention fraction increases gradually from ~ 0.4 to 0.7 as the cluster escape speed increases from ~ 10 to 100 km s^{-1} (Fig. 4). Tables 2–5 give the numbers of BHs in different kinds of systems, both retained in and ejected from clusters with different escape speeds. Their main properties are illustrated in Figures 5–8. Single BH masses can become as large as $\sim 100 M_{\odot}$ (as a consequence of massive binary mergers, especially if mass loss during mergers is small). These “intermediate-mass” BHs are almost always retained in clusters. If they were to acquire a new binary companion through dynamical interactions in the dense cluster environment, they could become ULXs. However, it was recently demonstrated that although massive BHs easily acquire binary companions, it is rather unlikely to find such a binary at high ultraluminous X-ray luminosity (Blecha et al. 2006).

BH–BH binaries (rather than double NSs), are probably the most promising GW sources for detection by ground-based interferometers (Lipunov, Postnov, & Prokhorov 1997; Bulik & Belczynski 2003). Merging BH–BH systems therefore are important sources for present projects to detect astrophysical GW sources (e.g., GEO, LIGO, VIRGO). The properties of BH–BH binaries in much

larger stellar systems with continuous star formation (e.g., disk galaxies) were studied extensively by Bulik & Belczynski (2003; Bulik, Belczynski & Rudak 2004a; Bulik, Gondek-Rosinska & Belczynski 2004b). We find that the properties of BH–BH binaries in starbursts are not too different from those found in previous studies. Most BH–BH systems are characterized by rather equal masses, with a mass ratio distribution peaking at $q \simeq 0.8 - 1.0$ (cf. the Pop II models of Bulik et al. 2004b). For most models only a small fraction (a few per cent; e.g., 5% for Model A) of the BH–BH systems are tight enough to merge within a Hubble time and produce observable GW signals. For models which tend to produce tighter BH–BH binaries (D and E), the fraction can be significantly higher ($\sim 10\text{--}40\%$). However, in Model E there are almost no BH–BH binaries, and the higher fraction of coalescing systems does not mean a higher BH–BH merger rate. Models C1 and D are the most efficient in producing merging BH–BH binaries: 2035 and 1370, respectively (for a total starburst mass of $\sim 10^8 M_{\odot}$; Table 1), while for most of the other models (including the reference model) we find $\sim 300\text{--}600$ merging BH–BH systems.

This work was supported in part by KBN grants PBZ-KBN-054/P03/2001 and 1 P03D 022 28 at the Copernicus Center, Poland, and by NSF Grant PHY-0245028 and NASA Grants NAG5-12044 and NAG5-13236 at Northwestern University. For hospitality and support, AS thanks the Astronomy Department at New Mexico State University and the Theoretical Astrophysics Group at Northwestern University; KB thanks the Aspen Center for Physics; and FAR thanks the Aspen Center for Physics and the Center for Gravitational Wave Physics at Penn State University.

REFERENCES

- Abt, H. A. 1983, *ARA&A*, 21, 343
 Arzoumanian, Z., Chernoff, D. F., & Cordes, J. M. 2002, *ApJ*, 568, 289
 Baumgardt, H., Hut, P., Makino, J., McMillan, S., & Portegies Zwart, S. 2003a, *ApJ*, 582, L21
 Baumgardt, H., Makino, J., Hut, P., McMillan, S., & Portegies Zwart, S. 2003b, *ApJ*, 589, L25
 Baumgardt, H., Makino, J., & Ebisuzaki, T. 2004, *ApJ*, 613, 1143
 Baumgardt, H., Makino, J., & Hut, P. 2005, *ApJ*, 620, 238
 Belczynski, K., Bulik, T., & Ruitter, A. 2005, *ApJ*, 629, 915
 Belczynski, K., Kalogera, V., & Bulik, T. 2002, *ApJ*, 572, 407 (BKB02)
 Belczynski, K., Kalogera, V., Rasio, F., Taam, R., Zezas, A., Bulik, T., Maccarone, T., & Ivanova, N. 2006, *ApJ*, submitted (astro-ph/0511811)
 Belczynski, K., Sadowski, A., & Rasio, F. 2004, *ApJ*, 611, 1068 (Paper I)
 Blecha, L., Ivanova, N., Kalogera, V., Belczynski, K., Fregeau, J., & Rasio, F. 2006, *ApJ*, 642, 427
 Bulik, T., & Belczynski, K. 2003, *ApJ*, 589, L37
 Bulik, T., Belczynski, K., & Rudak, B. 2004a, *A&A*, 415, 407
 Bulik, T., Gondek-Rosinska, D., & Belczynski, K. 2004b, *MNRAS*, 352, 1372
 Cropper, M., Soria, R., Mushotzky, R.F., Wu, K., Markwardt, C.B., Pakull, M. 2004, *MNRAS*, 349, 39
 Duquennoy, A., & Mayor, M. 1991, *A&A*, 248, 485
 Ebisuzaki, T., et al. 2001, *ApJ*, 562, L19
 Elmegreen, D.M., Chromey, F.R., McGrath, E.J., & Ostenson, J.M. 2002, *AJ*, 123, 1381
 Freitag, M., Rasio, F.A., & Baumgardt, H. 2006a, *MNRAS*, 368, 121
 Freitag, M., Gürkan, M.A., & Rasio, F.A. 2006b, *MNRAS*, 368, 141
 Fryer, C. L. 1999, *ApJ*, 522, 413
 Fryer, C. L., & Kalogera, V. 2001, *ApJ*, 554, 548
 Gebhardt, K., Rich, R.M., & Ho, L.C. 2002, *ApJ*, 578, L41
 Gebhardt, K., Rich, R.M., & Ho, L.C. 2005, *ApJ*, submitted
 Gerssen, J., van der Marel, R.P., Gebhardt, K., Guhathakurta, P., Peterson, R.C., & Pryor, C. 2002, *AJ*, 124, 3270
 Gerssen, J., van der Marel, R.P., Gebhardt, K., Guhathakurta, P., Peterson, R.C., & Pryor, C. 2003, *AJ*, 125, 376
 Gültekin, K., Miller, M.C., & Hamilton, D.P. 2004, *ApJ*, 616, 221
 Gürkan, M.A., Freitag, M., & Rasio, F.A. 2004, *ApJ*, 604, 632
 Häring, N., & Rix, H.-W. 2004, *ApJ*, 604, L89
 Heger, A., Fryer, C.L., Woosley, S.E., Langer, N., & Hartmann, D.H. 2003, *ApJ*, 591, 288
 Heggie, D. C. 1975, *MNRAS*, 173, 729
 Hurley, J. R., Pols, O. R., & Tout, C. A. 2000, *MNRAS*, 315, 543
 Hurley, J. R., Tout, C. A., & Pols, O. R. 2002, *MNRAS*, 329, 827
 Ivanova, N., Belczynski, K., Fregeau, J.M., & Rasio, F.A. 2005, *MNRAS*, 358, 572
 Kaaret, P., et al. 2001, *MNRAS*, 321, L29
 Kalogera, V. 1996, *ApJ*, 471, 352
 Kalogera, V., King, A.R., & Rasio, F.A. 2004, *ApJ*, 601, L171
 King, A.R. 2004, *MNRAS*, 347, L18
 King, A.R., Davies, M.B., Ward, M.J., Fabbiano, G., & Elvis, M. 2001, *ApJ*, 552, L109
 Kroupa, P., Tout, C.A., & Gilmore, G., 1993, *MNRAS*, 262, 545
 Kroupa, P., & Weidner, C. 2003, *ApJ*, 598, 1076
 Kulkarni, S.R., Hut, P., & McMillan, S. 1993, *Nature*, 364, 421
 Lipunov, V.M., Postnov, K.A., & Prokhorov, M.E. 1997, *NewA*, 2, 43
 McCrady, N., Gilbert, A.M., & Graham, J.R. 2003, *ApJ*, 596, 240
 Melo, V.P., Munoz-Tunon, C., Maiz-Apellaniz, J., & Tenorio-Tagle, G. 2005, *ApJ*, 619, 270; erratum 632, 684
 Miller, J.M., Fabbiano, G., Miller, M.C., & Fabian, A.C. 2003, *ApJ*, 585, L37
 Miller, M.C. 2002, *ApJ*, 581, 438
 Miller, M.C., & Colbert, E.J.M. 2004, *Int. J. Mod. Phys. D*, 13, 1
 Miller, M.C., & Hamilton, D.P. 2002, *MNRAS*, 330, 232
 Mirabel, I. F., & Rodrigues, I. 2003, *Science*, 300, 1119
 Nelemans, G., & Tout, C. A. 2005, *MNRAS*, 356, 753

- O'Leary, R.M., Rasio, F.A., Fregeau, J.M., Ivanova, N., & O'Shaughnessy, R. 2005, ApJ, in press [astro-ph/0508224]
- Podsiadlowski, P., Nomoto, K., Maeda, K., Nakamura, T., Mazzali, P., & Schmidt, B. 2002, ApJ, 567, 491
- Portegies Zwart, S.F. & McMillan, S.L.W. 2000, ApJ, 528, L17
- Portegies Zwart, S.F. & McMillan, S.L.W. 2002, ApJ, 576, 899
- Sigurdsson, S., & Hernquist, L. 1993, Nature, 364, 423
- Tauris, T.M., & Takens, R.J. 1998, A&A, 330, 1047
- van der Marel, R.P. 2004, in Coevolution of Black Holes and Galaxies, ed. L.C. Ho (Cambridge Univ. Press, Carnegie Obs. Ast. Ser. Vol. 1), 37
- Watters, W.A., Joshi, K.J., & Rasio, F.A. 2000, ApJ, 539, 331
- Webbink, R. F. 1984, ApJ, 277, 355
- Wheeler, J. C., Lecar, M., & McKee, C. F. 1975, ApJ, 200, 145
- White, N.E., & Van Paradijs, J. 1996, ApJ, 473, L25
- Willems, B., Henninger, M., Levin, T., Ivanova, N., Kalogera, V., McGhee, K., Timmes, F.X., & Fryer, C.L. 2005, ApJ, 625, 324
- Will, C.M. 2004, ApJ, 611, 1080
- Woosley, S.E. 1986, in 'Nucleosynthesis and Chemical Evolution', 16th Saas-Fee Course, ed. B. Hauck et al., Geneva Obs., 1
- Zezas, A., & Fabbiano, G. 2002, ApJ, 577, 726

TABLE 1
POPULATION SYNTHESIS MODEL ASSUMPTIONS

Model	Description ^a	Mass [M_{\odot}] in Single Stars	Mass [M_{\odot}] in Binaries
A	standard model described in § 2.4	3.79×10^7	5.95×10^7
B	uncorrelated binary component masses	3.79×10^7	7.59×10^7
C1-2	metallicity $Z = 0.0001, 0.02$	3.79×10^7	5.95×10^7
D	standard CE: $\alpha_{\text{CE}} \times \lambda = 0.1$	3.79×10^7	5.95×10^7
E	full kicks for BHs	3.79×10^7	5.95×10^7
F	steeper IMF: $\alpha_3 = -2.7$	5.97×10^7	9.49×10^7
G1	lower maximum mass: $M_{\text{max}} = 50M_{\odot}$	3.69×10^7	5.80×10^7
G2	lower maximum mass: $M_{\text{max}} = 100M_{\odot}$	3.75×10^7	5.88×10^7
H	$M_{\text{max,NS}} = 2M_{\odot}$	3.79×10^7	5.95×10^7
I ^b	BHs more massive than $10M_{\odot}$	3.79×10^7	5.95×10^7
J	alternative CE: $\gamma = 1.5$	3.79×10^7	5.95×10^7

^aDetails of model assumptions are given in § 2.4.

^bModel I is shown only to give the numbers of BHs (formed in the standard Model A) with mass greater than $10M_{\odot}$.

TABLE 2

BLACK HOLE POPULATIONS: RETAINED IN/EJECTED FROM CLUSTER^a WITH $V_{\text{esc}} = 10 \text{ km s}^{-1}$ - STANDARD MODEL

Type ^b	8.7 Myr $M_{\text{to}} = 25 M_{\odot}$	11.0 Myr $M_{\text{to}} = 20 M_{\odot}$	15.8 Myr $M_{\text{to}} = 15 M_{\odot}$	41.7 Myr $M_{\text{to}} = 8 M_{\odot}$	103.8 Myr $M_{\text{to}} = 5 M_{\odot}$
BH-MS	13113/4897	11444/5422	8622/4114	4696/2238	2941/1338
BH-HG	12/2	16/5	16/3	9/6	10/5
BH-RG	0/0	0/0	0/0	1/3	3/6
BH-CHeB	1193/72	945/116	634/68	270/16	175/25
BH-AGB	25/0	16/0	19/1	10/1	14/0
BH-He	79/142	29/107	10/90	7/281	0/388
BH-WD	0/0	0/0	0/9	37/396	1106/1163
BH-NS	0/62	0/370	2/793	11/999	16/967
BH-BH	8758/1880	9180/2252	9179/2257	9179/2247	9179/2226
Total in binaries:	23180 /7055	21630/8272	18482/7335	14220/6187	13444/6118
Single: binary disruption	2103/26501	3164/46773	3798/60129	3877/65384	3878/66190
Single: binary merger	5507/2236	7368/5452	13429/8342	15522/16234	15526/16300
Single progenitor	60015/16315	63030/43360	63030/55855	63030/55855	63030/55855
Total single:	67625/45052	73562/95585	80257/124326	82429/137473	82434 /138345

^aRetained populations contain all BHs with $V_{\text{bh}} < V_{\text{esc}}$ while ejected populations include BHs with $V_{\text{bh}} \geq V_{\text{esc}}$

^bBlack holes in binary systems are listed according to their companion types: MS—main sequence, HG—Hertzsprung Gap, RG—reg giant, CHeB—core He burning, AGB—asymptotic giant branch, He—helium star, WD—white dwarf, NS—neutron star, BH—black hole. Single black holes formed from components of disrupted binaries are listed under “Single: binary disruption.” Single black holes formed from binary merger products are under “Single: binary merger.” Single black holes that are remnants of single stars are listed under “Single progenitor.”

TABLE 3

BLACK HOLE POPULATIONS: RETAINED IN/EJECTED FROM CLUSTER^a WITH $V_{\text{esc}} = 50 \text{ km s}^{-1}$ - STANDARD MODEL

Type	8.7 Myr $M_{\text{to}} = 25 M_{\odot}$	11.0 Myr $M_{\text{to}} = 20 M_{\odot}$	15.8 Myr $M_{\text{to}} = 15 M_{\odot}$	41.7 Myr $M_{\text{to}} = 8 M_{\odot}$	103.8 Myr $M_{\text{to}} = 5 M_{\odot}$
BH-MS	15616/2394	14055/2811	10357/2379	5382/1552	3317/962
BH-HG	14/0	20/1	19/0	11/4	11/4
BH-RG	0/0	0/0	0/0	1/3	4/5
BH-CHeB	1261/4	1057/4	697/5	284/2	187/13
BH-AGB	25/0	16/0	20/0	11/0	14/0
BH-He	204/17	123/13	86/14	117/171	45/343
BH-WD	0/0	0/0	0/9	274/159	1682/587
BH-NS	1 /61	11/359	66/729	173/837	181/802
BH-BH	9787/851	10410/1022	10415/1021	10415/1011	10415/990
Total in binaries:	26908/3327	25692/4210	21660/4157	16668/3739	15856/3706
Single: binary disruption	10775/17829	18136/31801	22195/41732	22848/46413	22900/47168
Single: binary merger	6804/939	9906/2914	17059/4722	20625/11131	20630/11196
Single progenitor	65230/11100	75465/30925	75830/42585	75830/42585	75830/42585
Total single:	82809/29868	103507/65640	115084/89039	119303/100129	119360/100949

^a Same as Table 2.

TABLE 4
BLACK HOLE POPULATIONS: RETAINED IN/EJECTED FROM CLUSTER^a WITH $V_{\text{esc}} = 100 \text{ km s}^{-1}$ -
STANDARD MODEL

Type ^a	8.7 Myr $M_{\text{to}} = 25 M_{\odot}$	11.0 Myr $M_{\text{to}} = 20 M_{\odot}$	15.8 Myr $M_{\text{to}} = 15 M_{\odot}$	41.7 Myr $M_{\text{to}} = 8 M_{\odot}$	103.8 Myr $M_{\text{to}} = 5 M_{\odot}$
BH-MS	17163/847	15857/1009	11794/942	6178/756	3722/557
BH-HG	14/0	21/0	19/0	15/0	12/3
BH-RG	0/0	0/0	0/0	2/2	7/2
BH-CHeB	1265/0	1061/0	702/0	286/0	190/10
BH-AGB	25/0	16/0	20/0	11/0	14/0
BH-He	215/6	131/5	97/3	252/36	222/166
BH-WD	0/0	0/0	1/8	388/45	2141/128
BH-NS	3/59	74/296	295/500	493/517	500/483
BH-BH	10224/414	10933/499	10942/494	10942/484	10939/466
Total in binaries:	28909/1326	28093/1809	23870/1947	18567/1840	17747/1815
Single: binary disruption	16165/12439	27776/22161	34536/29391	35981/33260	36155/33913
Single: binary merger	7244/499	11091/1729	18979/2802	24237/7519	24251/7575
Single progenitor	68465/7865	84455/21935	86245/32170	86245/32170	86245/32170
Total single:	91874/20803	123322/45825	139760/64363	146463/72949	146651/73658

^a Same as Table 2.

TABLE 5
BLACK HOLE POPULATIONS: RETAINED IN/EJECTED FROM CLUSTER^a WITH $V_{\text{esc}} = 300 \text{ km s}^{-1}$ -
STANDARD MODEL

Type ^a	8.7 Myr $M_{\text{to}} = 25 M_{\odot}$	11.0 Myr $M_{\text{to}} = 20 M_{\odot}$	15.8 Myr $M_{\text{to}} = 15 M_{\odot}$	41.7 Myr $M_{\text{to}} = 8 M_{\odot}$	103.8 Myr $M_{\text{to}} = 5 M_{\odot}$
BH-MS	17948/62	16780/86	12648/88	6845/89	4192/87
BH-HG	14/0	21/0	19/0	15/0	14/1
BH-RG	0/0	0/0	0/0	4/0	9/0
BH-CHeB	1265/0	1061/0	702/0	286/0	200/0
BH-AGB	25/0	16/0	20/0	11/0	14/0
BH-He	221/0	136/0	100/0	288/0	388/0
BH-WD	0/0	0/0	8/1	432/1	2266/3
BH-NS	54/8	339/31	755/40	979/31	960/23
BH-BH	10621/17	11400/32	11406/30	11399/27	11382/23
Total in binaries:	30148/87	29753/149	25658/159	20259/148	19425/137
Single: binary disruption	25364/3240	43111/6826	53392/10535	56379/12882	56789/13279
Single: binary merger	7703/40	12433/387	21100/681	28682/3074	28739/3087
Single progenitor	74140/2190	98615/7775	104050/14365	104050/14365	104050/14365
Total single:	107207/5470	154159/14988	178542/25581	189111/30321	189578/30731

^a Same as Table 2.

TABLE 6
RETAINED BH FRACTIONS FOR VARIOUS MODELS^a

Model	$f_{\text{bin}=0\%}$	$f_{\text{bin}=50\%}$	$f_{\text{bin}=100\%}$
A: 10 kms^{-1}	.53	.40	.27
A: 50 kms^{-1}	.64	.56	.49
A: 100 kms^{-1}	.73	.69	.64
A: 300 kms^{-1}	.88	.87	.86
B: 50 kms^{-1}	.64	.64	.63
C1: 50 kms^{-1}	.74	.64	.54
C2: 50 kms^{-1}	.42	.49	.56
D: 50 kms^{-1}	.64	.59	.54
E: 50 kms^{-1}	.02	.16	.29
F: 50 kms^{-1}	.61	.54	.46
G1: 50 kms^{-1}	.56	.50	.43
G2: 50 kms^{-1}	.63	.55	.47
H: 50 kms^{-1}	.52	.47	.42
I: 50 kms^{-1}	.81	.73	.63
J: 50 kms^{-1}	.64	.56	.49

^aFractions are calculated for entire BH population; both single and binary BHs added with the assumed initial cluster binary fraction f_{bin} . The fractions are obtained for a time of 103.8 Myr after the starburst. For our (standard) Model A we show fractions for different escape velocities, while for all other models we assume $V_{\text{esc}} = 50 \text{ km s}^{-1}$.

TABLE 7
 VERY YOUNG BLACK HOLE POPULATIONS RETAINED IN/EJECTED FROM CLUSTER WITH $V_{\text{esc}} = 50 \text{ km s}^{-1}$ FOR
 DIFFERENT MODELS^a

Type	A	B	C1	C2	D	E
Binaries:						
BH-MS	14055/2811	30786/2331	23471/2489	2702/62	12147/730	1030/2342
BH-HG	20/1	0/0	43/0	3/0	23/0	2/0
BH-RG	0/0	0/0	0/0	0/0	0/0	0/0
BH-CHeB	1057/4	11/0	1624/7	179/0	943/0	51/6
BH-AGB	16/0	0/0	19/0	5/0	14/0	0/0
BH-He	123/13	0/0	365/3	84/0	37/0	53/7
BH-WD	0/0	0/0	0/0	0/0	0/0	0/0
BH-NS	11/359	0/3	41/630	67/30	11/127	0/192
BH-BH	10410/1022	24/3	22120/1121	4098/21	10149/1401	43/272
Total:	25692/4210	30821/2337	47683/4250	7138/113	23324/2258	1179/2819
Single:						
binary disruption	18136/31801	5067/14023	7317/16957	27101/30609	17544/23045	15978/75191
binary merger	9906/2914	5270/1881	8246/2243	9423/1654	10232/2123	8412/2732
Single progenitor	75465/30925	75465/30925	97745/17350	42580/59425	75465/30925	1820/105340
Total:	103507/65640	85802/46829	113308/36550	79104/91688	103241/56093	26210/183263
Type	F	G1	G2	H	I	J
Binaries:						
BH-MS	8046/1682	10925/2721	14692/2921	14203/4110	11346/9	13960/983
BH-HG	10/0	24/0	32/1	20/1	17/0	11/0
BH-RG	0/0	0/0	0/0	0/0	0/0	0/0
BH-CHeB	594/6	747/6	1056/6	1089/4	919/0	1061/0
BH-AGB	7/0	14/0	12/0	16/0	16/0	23/0
BH-He	87/5	105/8	128/13	126/19	19/0	86/3
BH-WD	0/0	0/0	0/0	0/0	0/0	0/0
BH-NS	0/207	4/324	7/404	1/75	0/0	9/265
BH-BH	4858/552	2885/634	8719/1024	10420/1353	10085/477	10568/927
Total:	13602/2452	14704/3693	24646/4369	25875/5562	22402/486	25718/2178
Single:						
binary disruption	10272/18773	14656/27049	19631/34003	18582/36967	10343/11915	20599/36724
binary merger	4325/1233	3132/1728	7816/2625	10413/3329	8720/1151	8823/1592
Single progenitor	43870/19615	54695/30545	71515/31090	75465/30925	68845/16640	75465/30925
Total:	58467/39621	72483/59322	98962/67718	104460/71221	87908/29706	104887/69241

^aAll numbers correspond to an age of 11 Myrs ($M_{\text{to}} = 20M_{\odot}$)

TABLE 8
 YOUNG BLACK HOLE POPULATIONS RETAINED IN/EJECTED FROM CLUSTER WITH $V_{\text{esc}} = 50 \text{ km s}^{-1}$ FOR DIFFERENT MODELS^a

Type	A	B	C1	C2	D	E
Binaries:						
BH-MS	3317/962	30116/2261	5448/774	816/45	3039/98	72/789
BH-HG	11/4	6/1	26/4	1/1	4/1	0/9
BH-RG	4/5	1/0	0/2	0/0	0/0	0/2
BH-CHeB	187/13	43/1	285/4	59/0	156/5	2/13
BH-AGB	14/0	4/0	24/0	0/0	11/0	0/0
BH-He	45/343	11/29	203/292	3/3	59/226	17/259
BH-WD	1682/587	235/36	3119/623	491/7	1431/139	201/506
BH-NS	181/802	5/7	651/1498	113/48	95/236	45/415
BH-BH	10415/990	24/3	22068/974	4097/20	10146/970	44/266
Total:	15856/3706	30445/2338	31824/4171	5580/124	14941/1675	381/2259
Single:						
binary disruption	22900/47168	5509/18263	12414/39071	29358/33357	22179/37215	19871/83178
binary merger	20530/11096	11740/6853	18390/10512	20127/10275	27122/15666	19417/10535
Single progenitor	75830/42585	75830/42585	92325/32465	42580/59425	75830/42585	2010/117555
Total:	119360/100949	93079/67701	123129/82048	92065/103057	125131/95466	41298/221268
Type	F	G1	G2	H	I	J
Binaries:						
BH-MS	1890/578	2522/938	3483/979	3319/1482	2952/8	3493/622
BH-HG	1/6	2/9	3/11	11/5	10/0	7/2
BH-RG	0/4	1/4	0/5	4/6	3/0	2/0
BH-CHeB	103/8	127/5	173/14	187/13	181/2	188/8
BH-AGB	8/0	10/0	12/0	14/0	14/0	11/0
BH-He	32/215	38/325	63/362	45/378	1/27	18/50
BH-WD	961/308	1401/560	1879/577	1743/629	1094/9	1609/199
BH-NS	87/502	132/738	185/929	165/755	40/21	129/718
BH-BH	4866/537	2898/613	8732/1000	10441/1434	10103/502	10578/896
Total:	7948/2158	7131/3192	14530/3877	15929/4702	14398/569	16035/2495
Single:						
binary disruption	13547/28403	19435/40297	24946/50147	28917/72295	12821/20559	25774/52599
binary merger	11225/7522	13100/9913	18325/11120	21892/13710	16923/4345	16475/6738
Single progenitor	44115/28245	55075/42620	71870/42440	76280/70605	68845/16640	75830/42585
Total:	68887/64170	87610/92830	115141/103707	127089/156610	98589/41544	118079/101922

^aAll numbers correspond to an age of 103.8 Myrs ($M_{\text{to}} = 5M_{\odot}$)

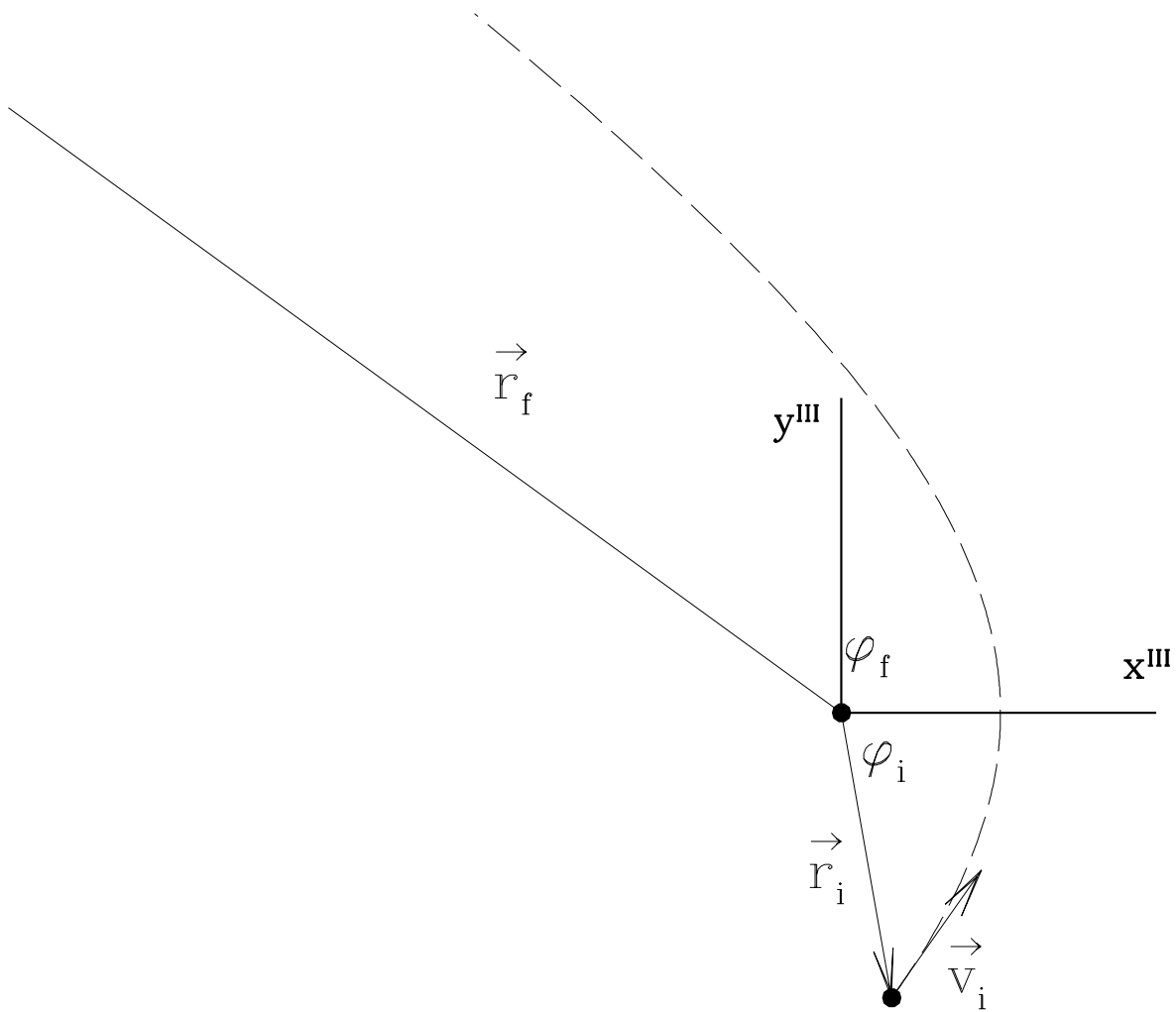


FIG. 1.— The trajectory of the newly born compact object in the system connected with the companion. For details see §2.3.

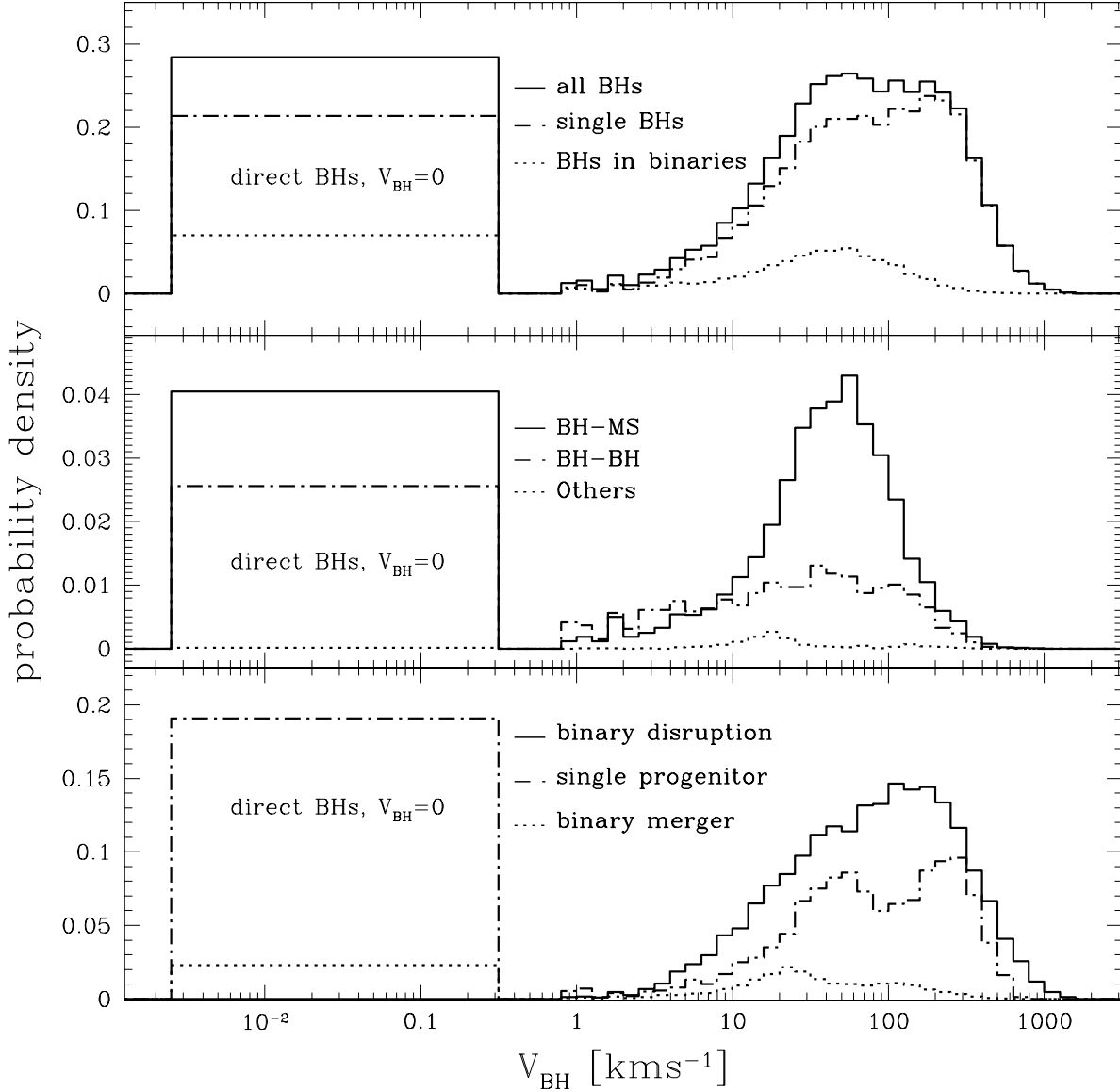


FIG. 2.— Spatial velocities of black holes at $t = 8.7 \text{ Myr}$ after the starburst. Overall distributions (all, single, binary BHs) are shown in the top panel. Middle panel shows various binary BH systems, while bottom panel shows the single BH populations. Note generally higher systemic speeds for single BHs. All curves are normalized to the total number of BHs at a given time (the distributions show $dN/d \log V_{\text{BH}}$). The no-kick BHs (direct formation) are contained in the left rectangular area. The area of the rectangle illustrates the relative numbers of no-kick and high-velocity systems.

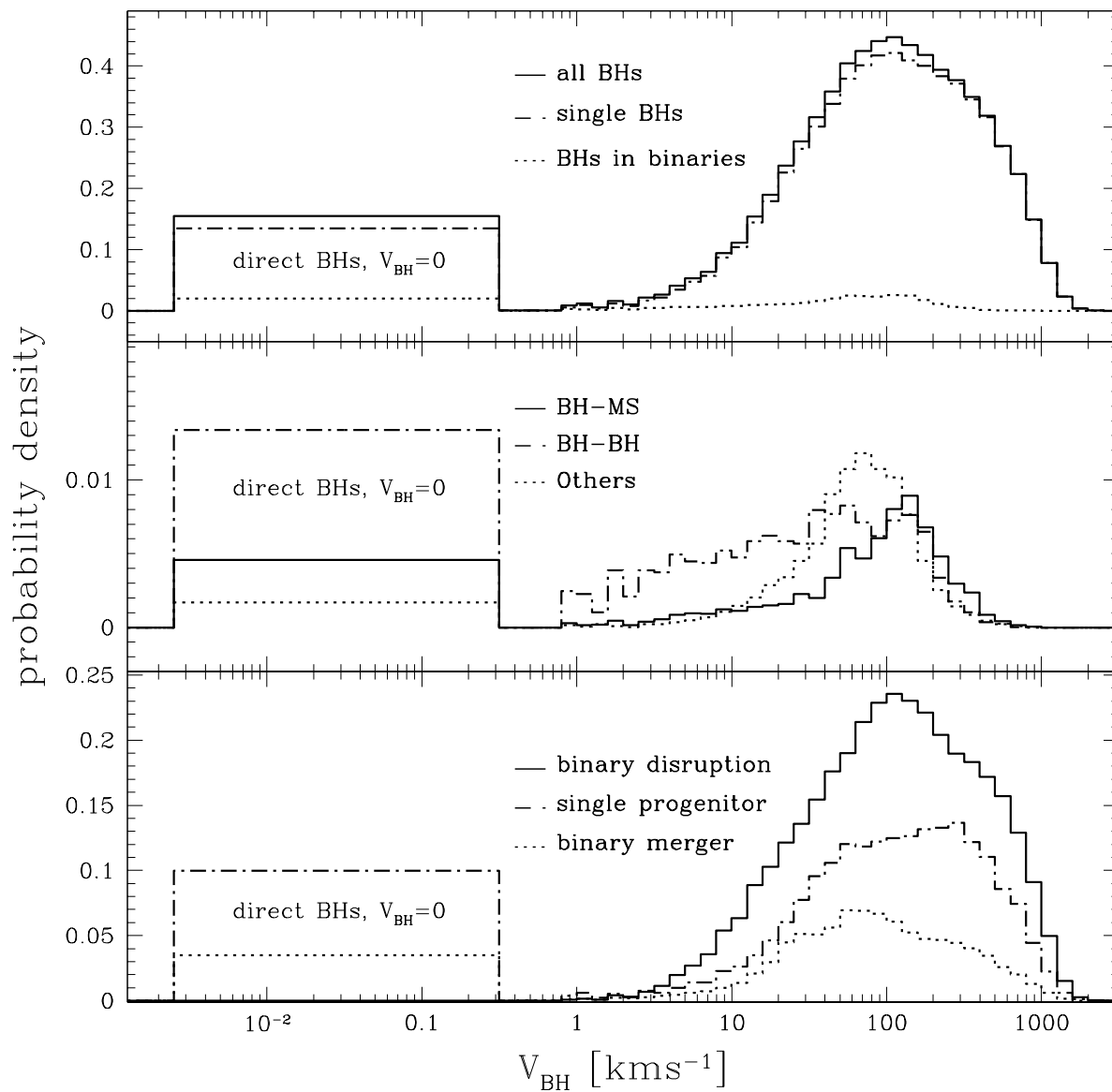


FIG. 3.— Spatial velocities of black holes at $t = 103.8 \text{ Myr}$ after the starburst. Lines same as for Fig. 2.

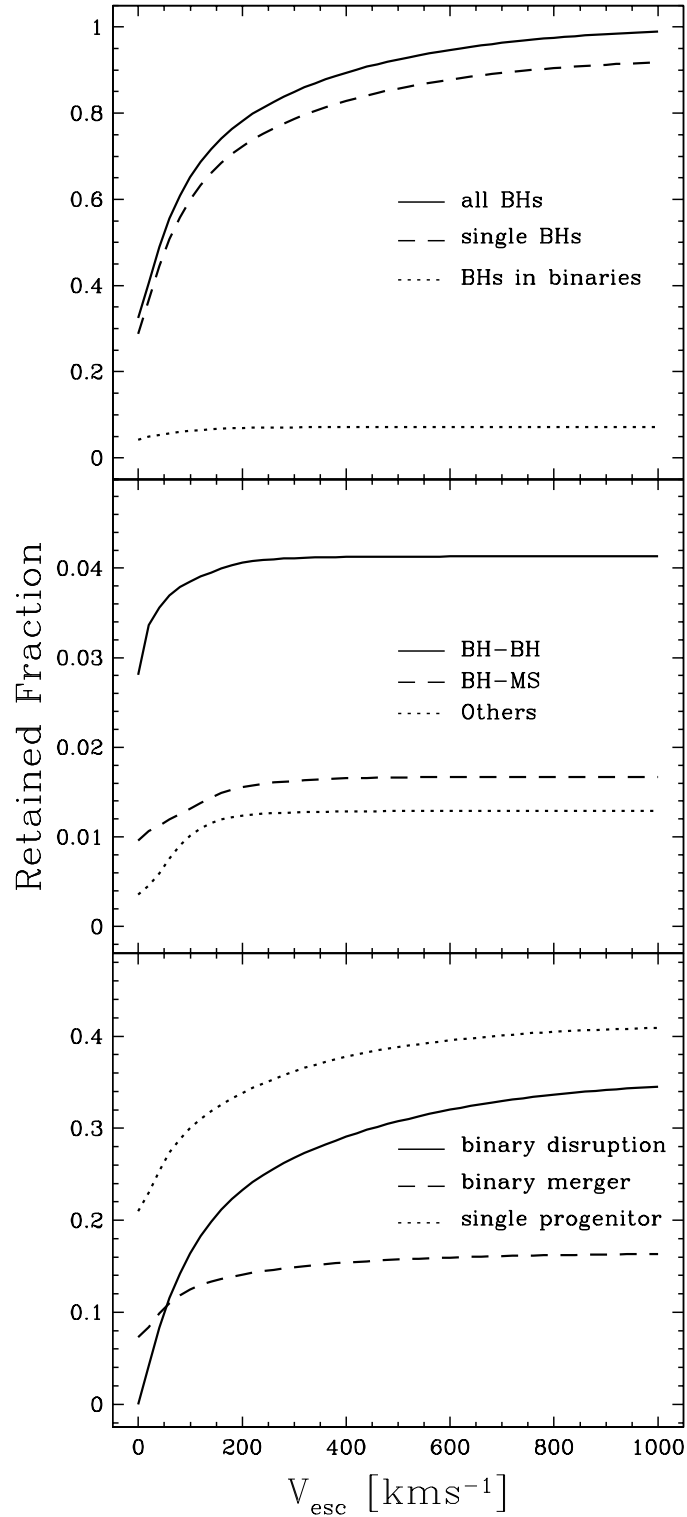


FIG. 4.— Retained fraction (cluster population) of BHs as a function of V_{esc} for our standard model at $t = 103.8$ Myr. Top panel shows overall population with contributions of single and binary BHs. Middle and bottom panels show various subpopulations of binary and single BHs, respectively. All curves are normalized to total number of BHs (single and binaries) formed in the standard model simulation.

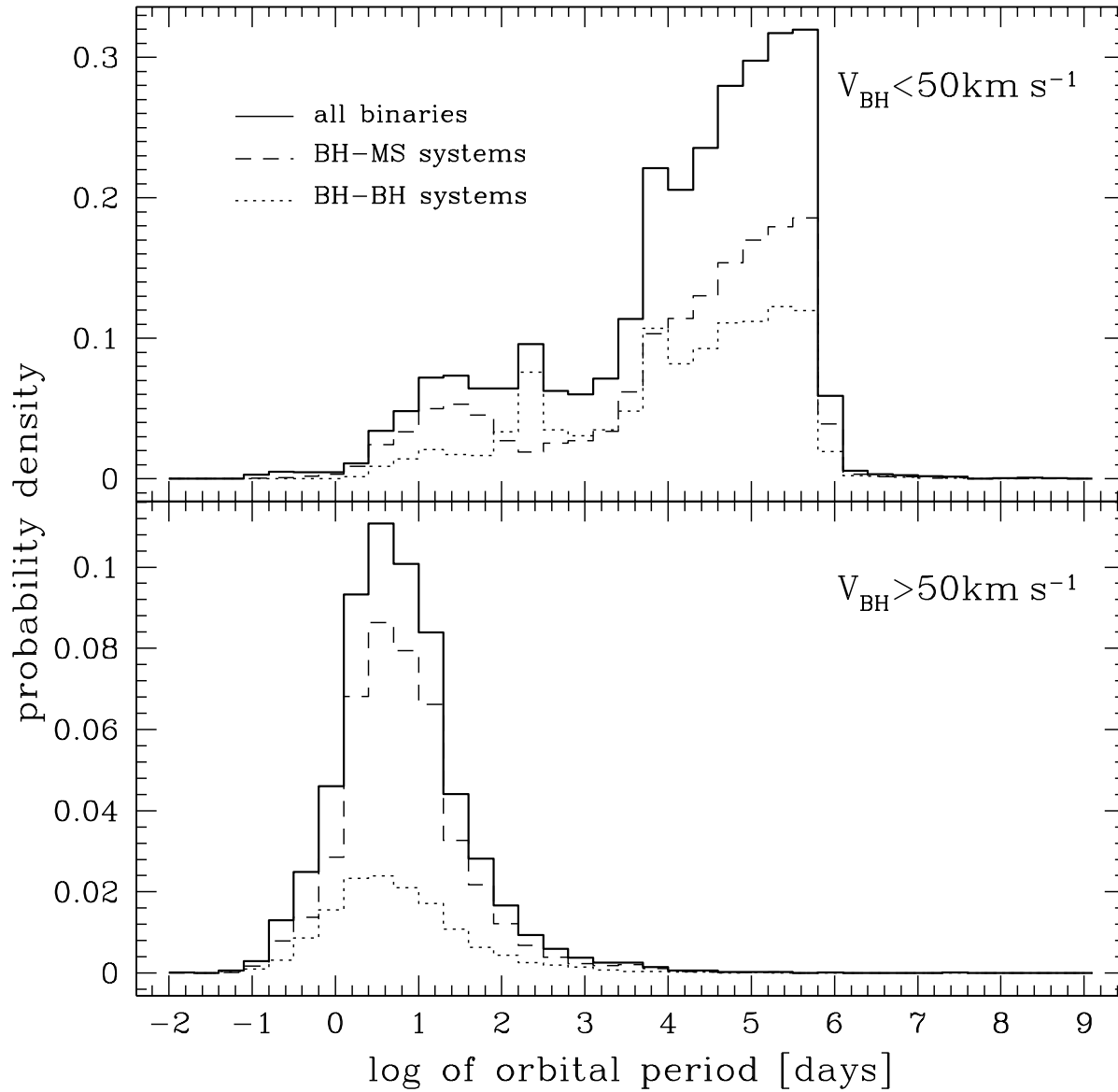


FIG. 5.— Period distribution of BH binaries retained in/ejected from cluster with $V_{\text{esc}} = 50 \text{ km s}^{-1}$ at 11 Myr for standard model. Two major contributing system types are shown separately: BH-MS binaries (dashed line) and BH-BH binaries (dotted line). All curves are normalized to total number of BHs (single and binaries). The distributions show $dN/d \log P_{\text{orb}}$. Note the different vertical scale on the panels.

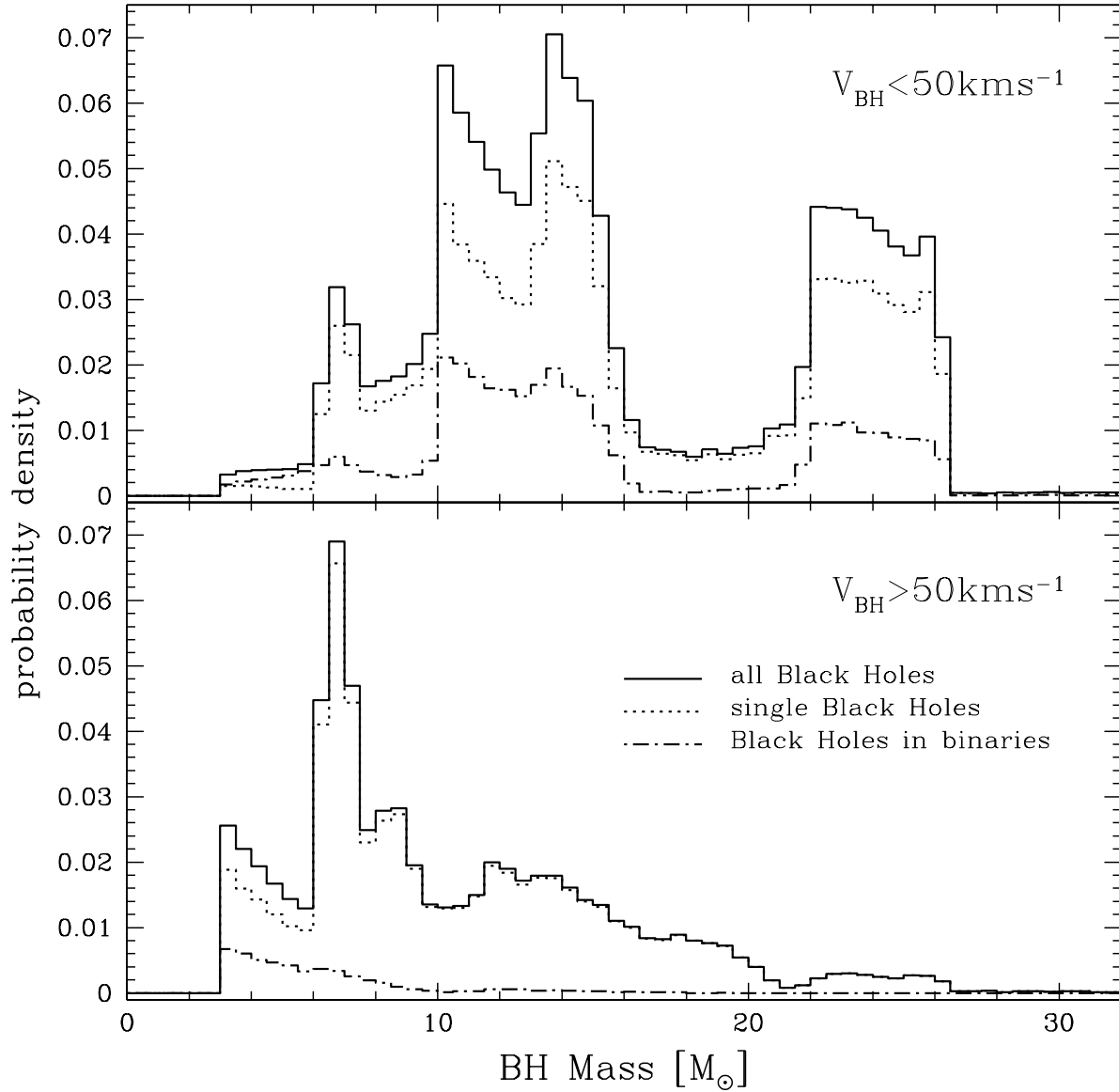


FIG. 6.— Mass distribution of BHs retained in/ejected from cluster with $V_{\text{esc}} = 50 \text{ km s}^{-1}$ at 11 Myr for standard model. Overall distribution is shown with a solid line, while single BHs are shown with a dotted line and BHs in binaries with a dashed line. All curves are normalized to total number of BHs (single and binaries).

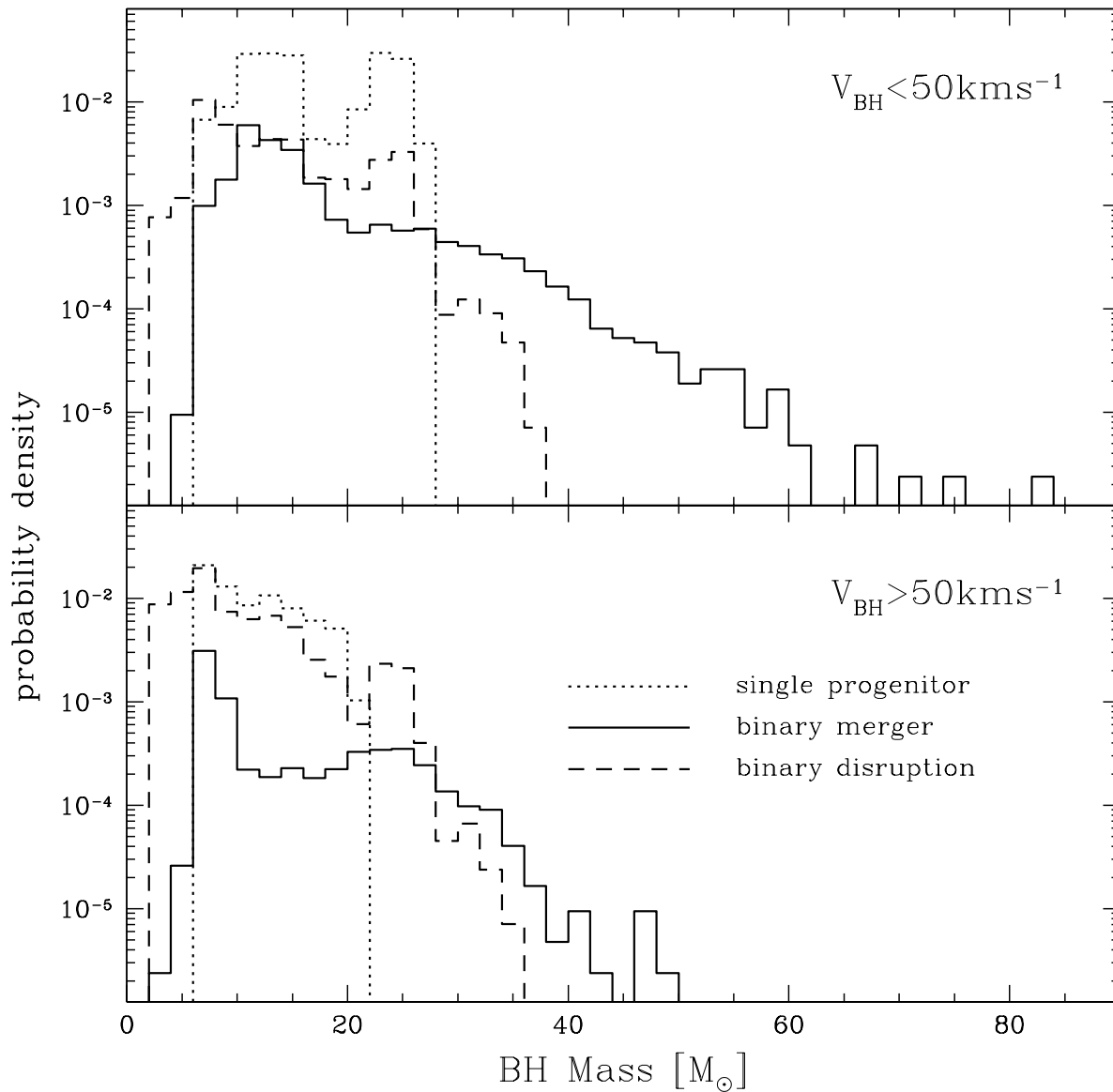


FIG. 7.— Mass distributions of various kinds of single BHs retained in/ejected from cluster with $V_{\text{esc}} = 50 \text{ km s}^{-1}$ at 11 Myr for standard model. The dotted line shows BHs originating from primordial single stars; the dashed line represents single BHs from disrupted binaries; the solid line is for single BHs that are remnants of merged binaries. All curves are normalized to total number of BHs (single and binaries). Note that, in contrast to Fig. 6, a logarithmic scale is used and the entire range of BH masses is shown.

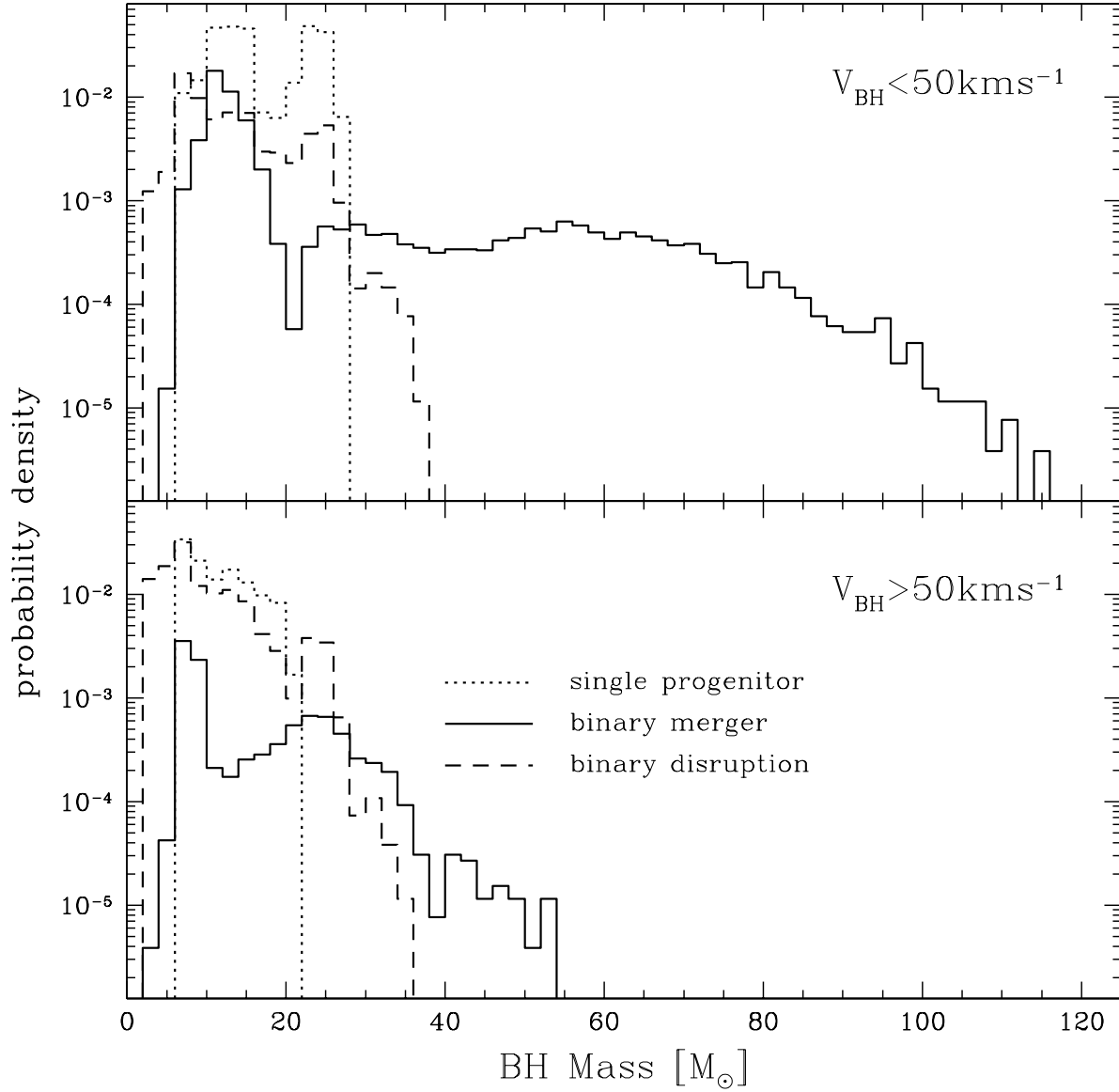


FIG. 8.— Same as Fig. 7 but for model in which the merger mass is calculated from the total mass of two merging binary components. See § 3.1.3 for details.

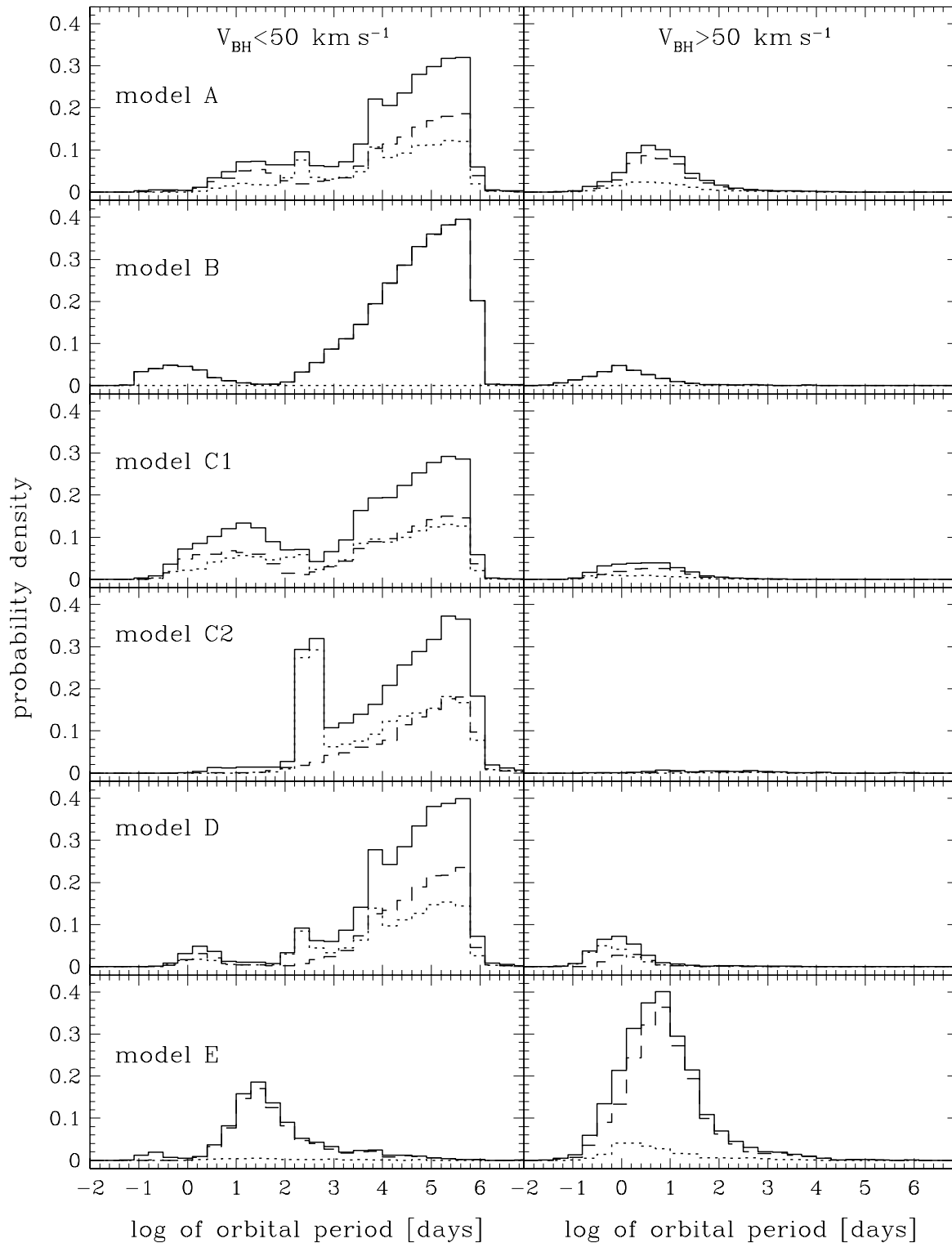


FIG. 9.— Period distribution of BH binaries retained in/ejected from cluster with $V_{\text{esc}} = 50 \text{ km s}^{-1}$ at 11 Myr for models A – E. Notations are the same as in Fig. 5.

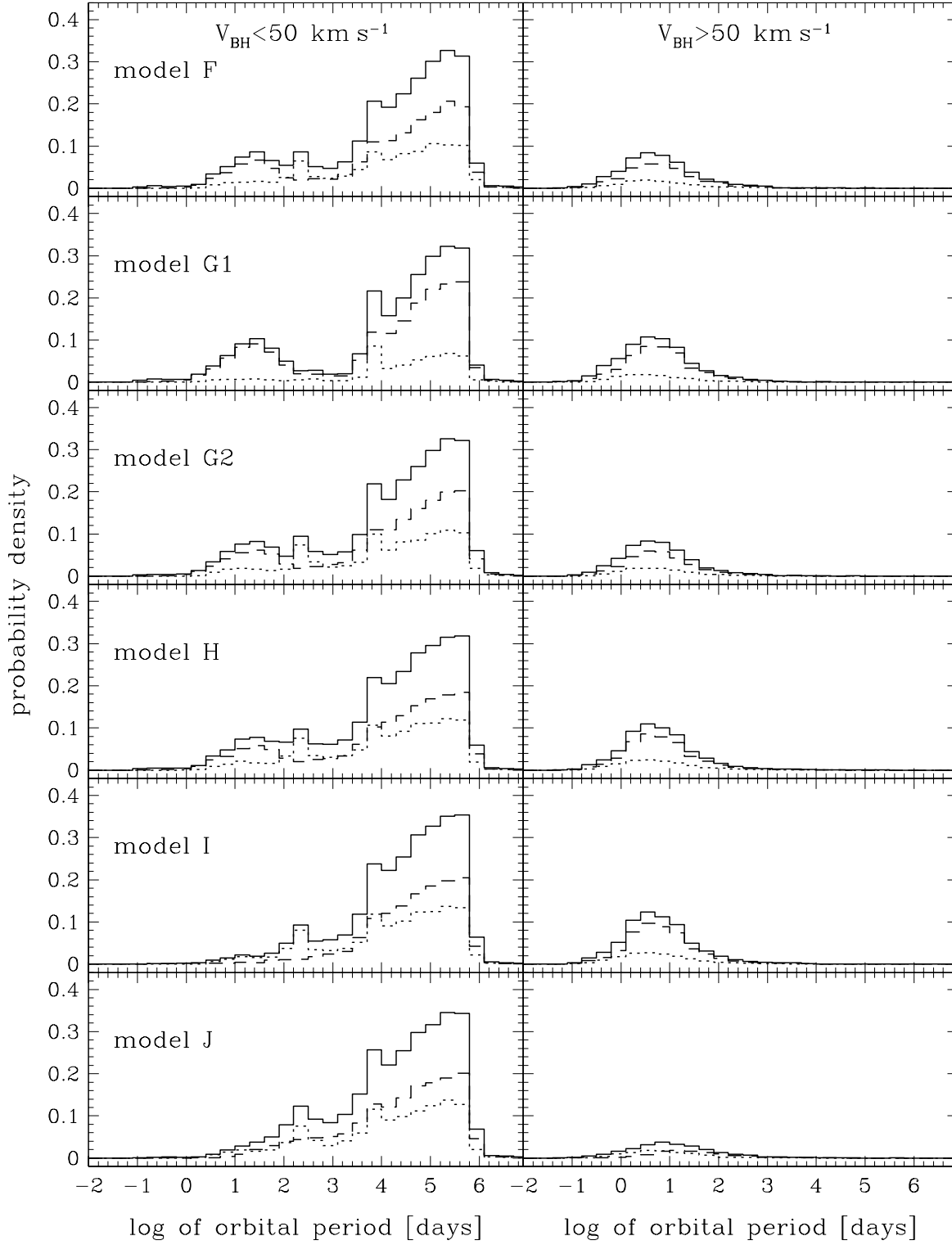


FIG. 10.— Period distribution of BH binaries retained in/ejected from cluster with $V_{\text{esc}} = 50 \text{ km s}^{-1}$ at 11 Myr for models F – J. Notations are the same as in Fig. 5.

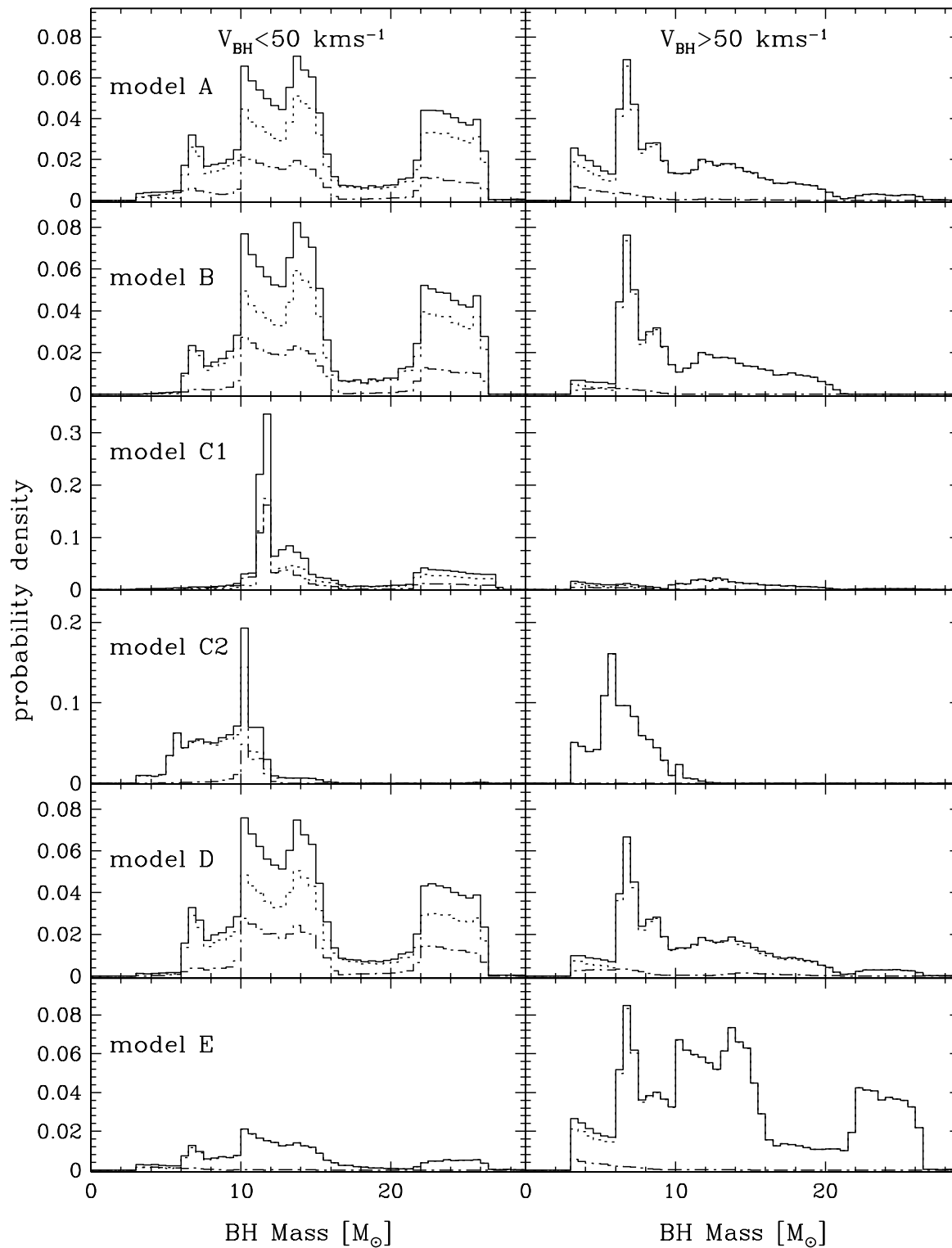


FIG. 11.— Mass distribution of BHs retained in/ejected from cluster with $V_{\text{esc}} = 50 \text{ km s}^{-1}$ at 11 Myr for models A – E. Notations are the same as in Fig. 6.

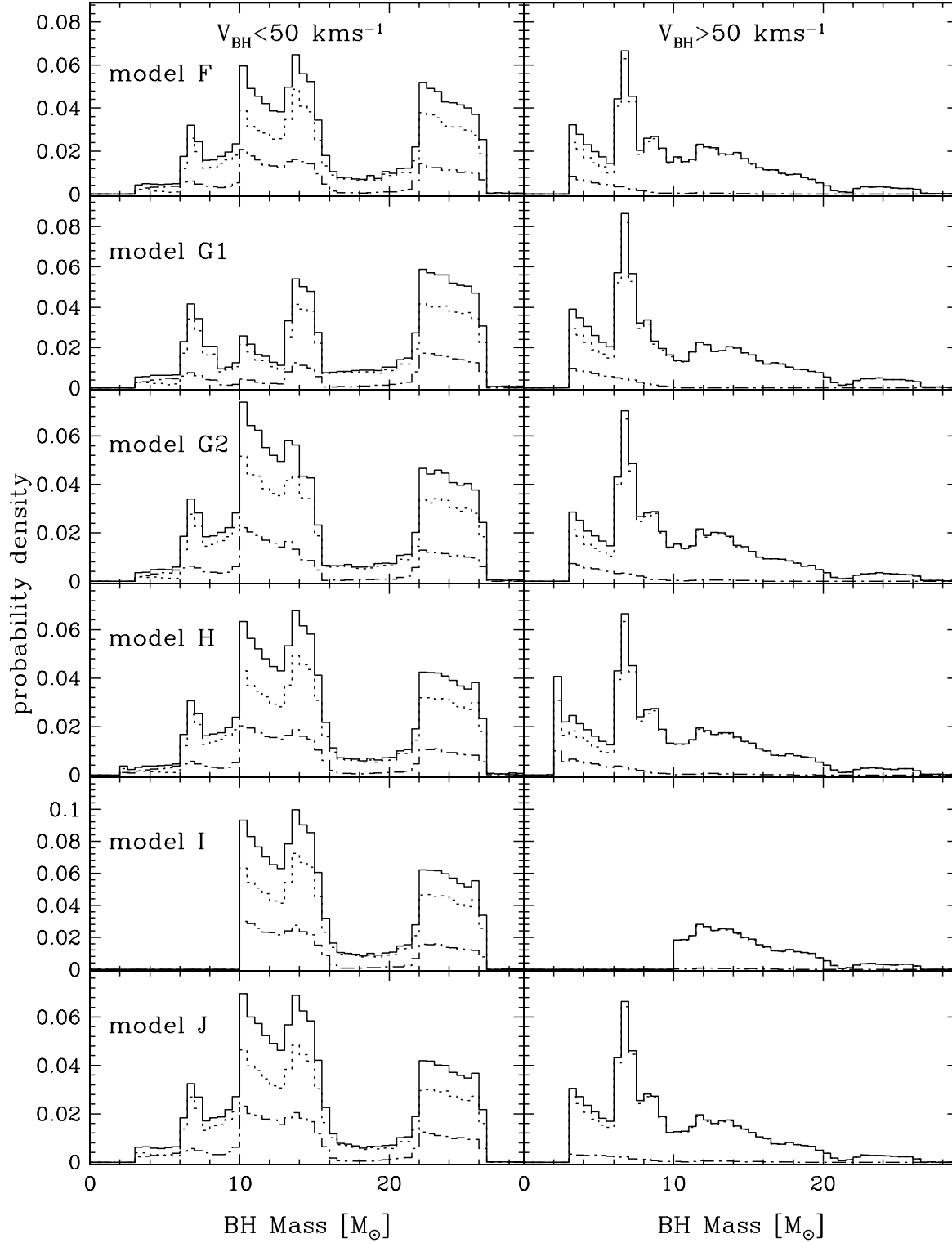


FIG. 12.— Mass distribution of BHs retained in/ejected from cluster with $V_{\text{esc}} = 50 \text{ km s}^{-1}$ at 11 Myr for models F – J. Notations are the same as in Fig. 6.

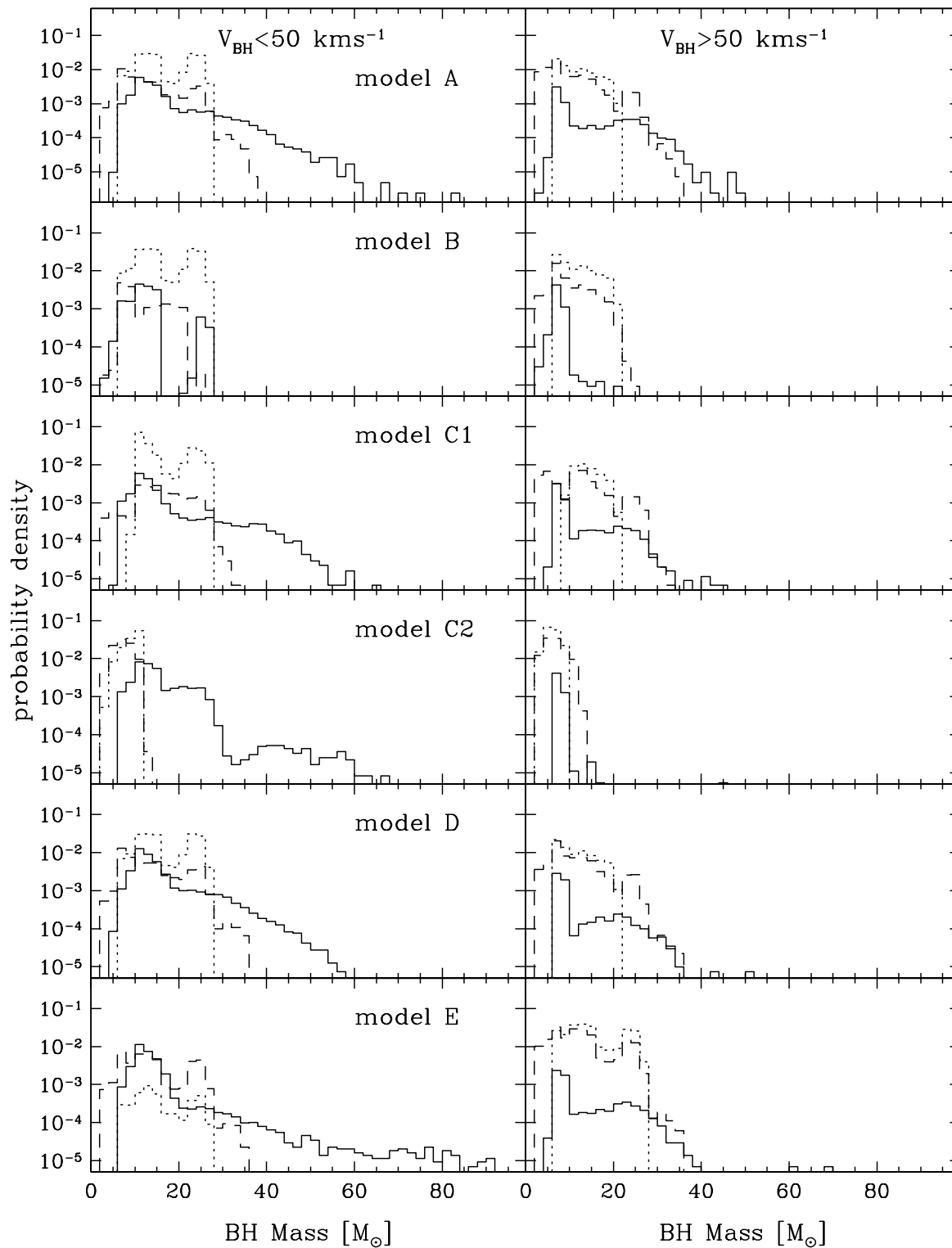


FIG. 13.— Mass distributions of various kinds of single BHs retained in/ejected from cluster with $V_{\text{esc}} = 50 \text{ km s}^{-1}$ at 11 Myr for models A – E. Notations are the same as in Fig. 7.

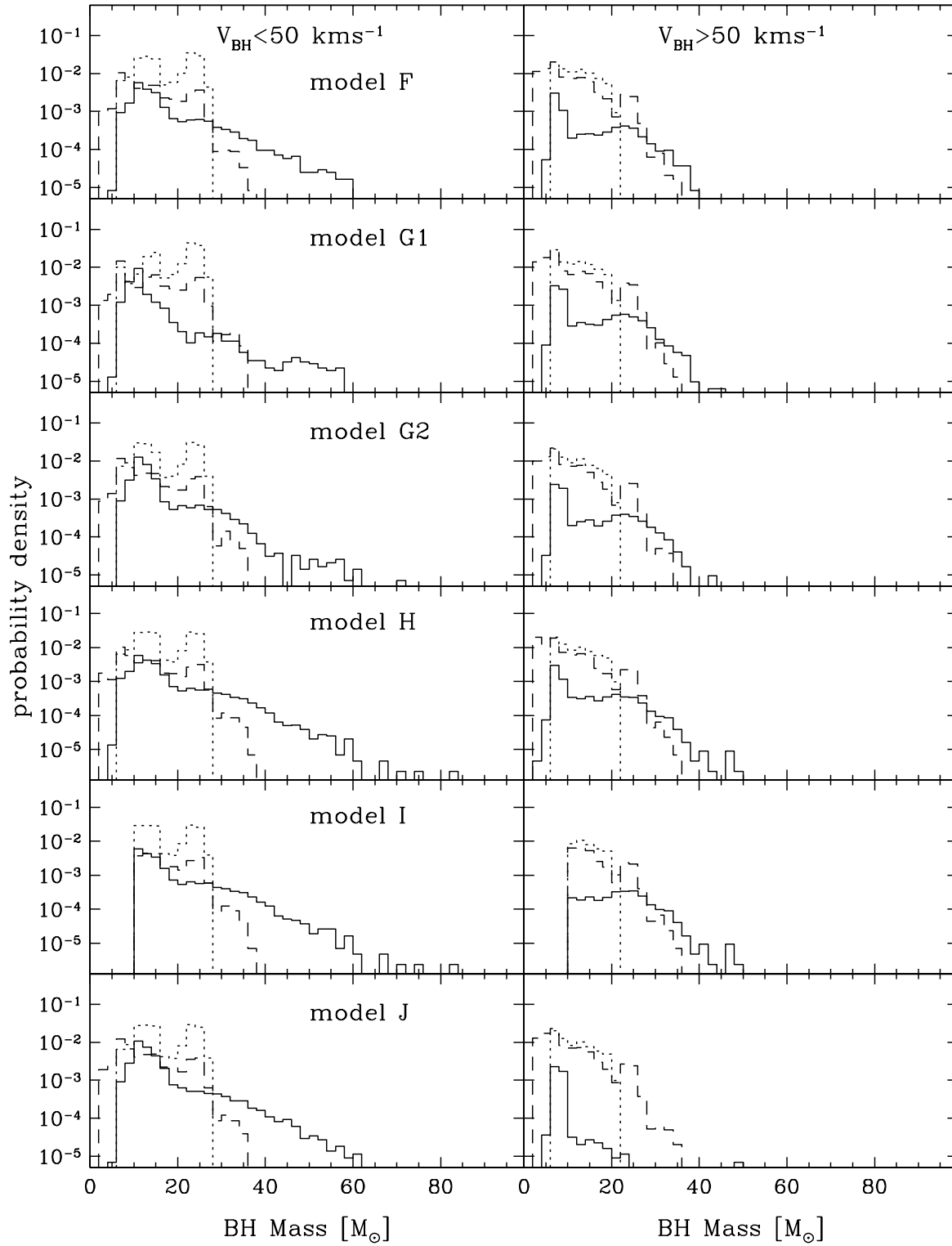


FIG. 14.— Mass distributions of various kinds of single BHs retained in/ejected from cluster with $V_{\text{esc}} = 50 \text{ km s}^{-1}$ at 11 Myr for models F – J. Notations are the same as in Fig. 7.

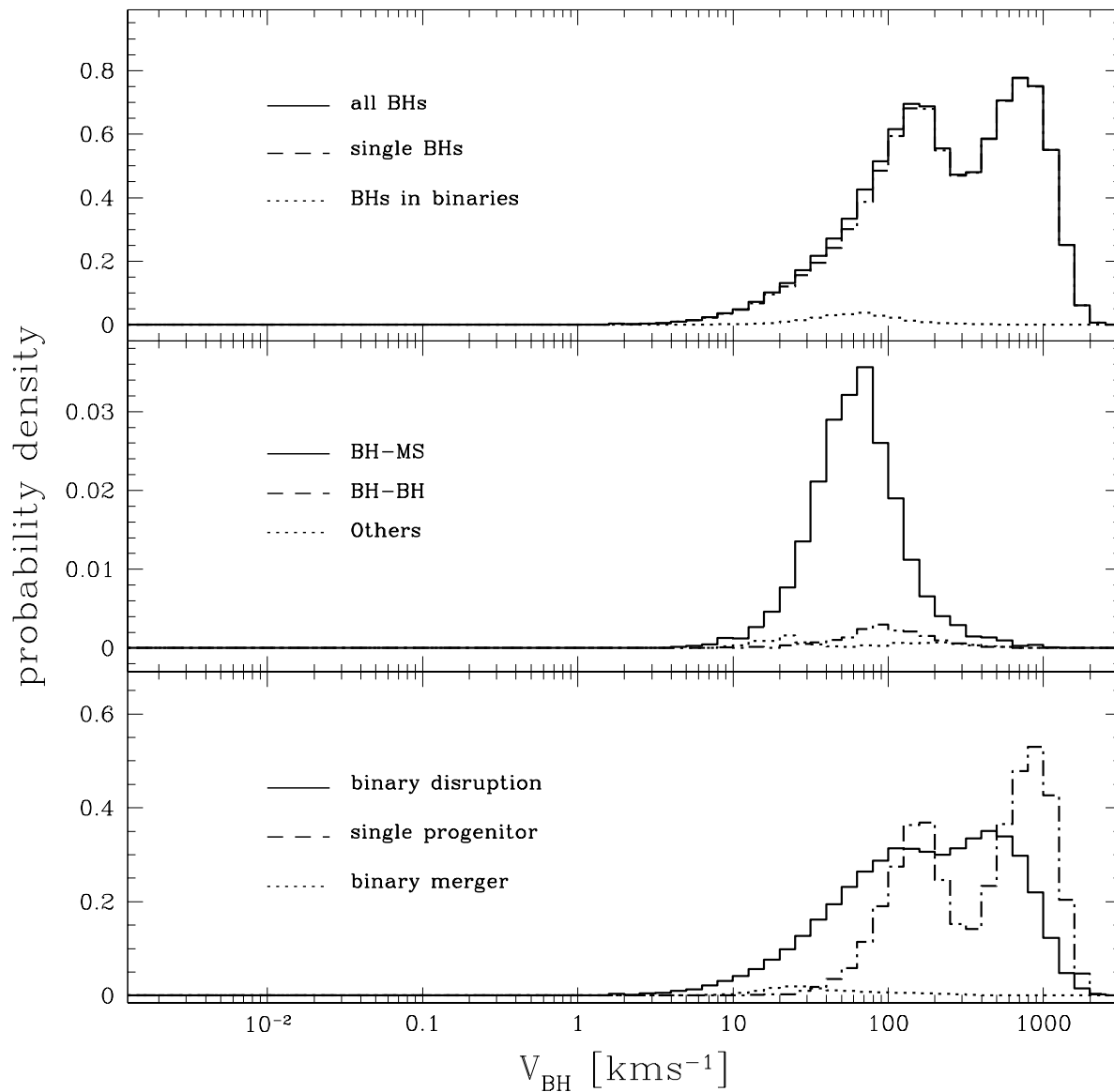


FIG. 15.— Spatial velocities of black holes at $t = 8.7 \text{ Myr}$ after the starburst for Model E. Lines same as for Fig. 2. Note absence of the no-kick BHs (cf. Fig. 2).

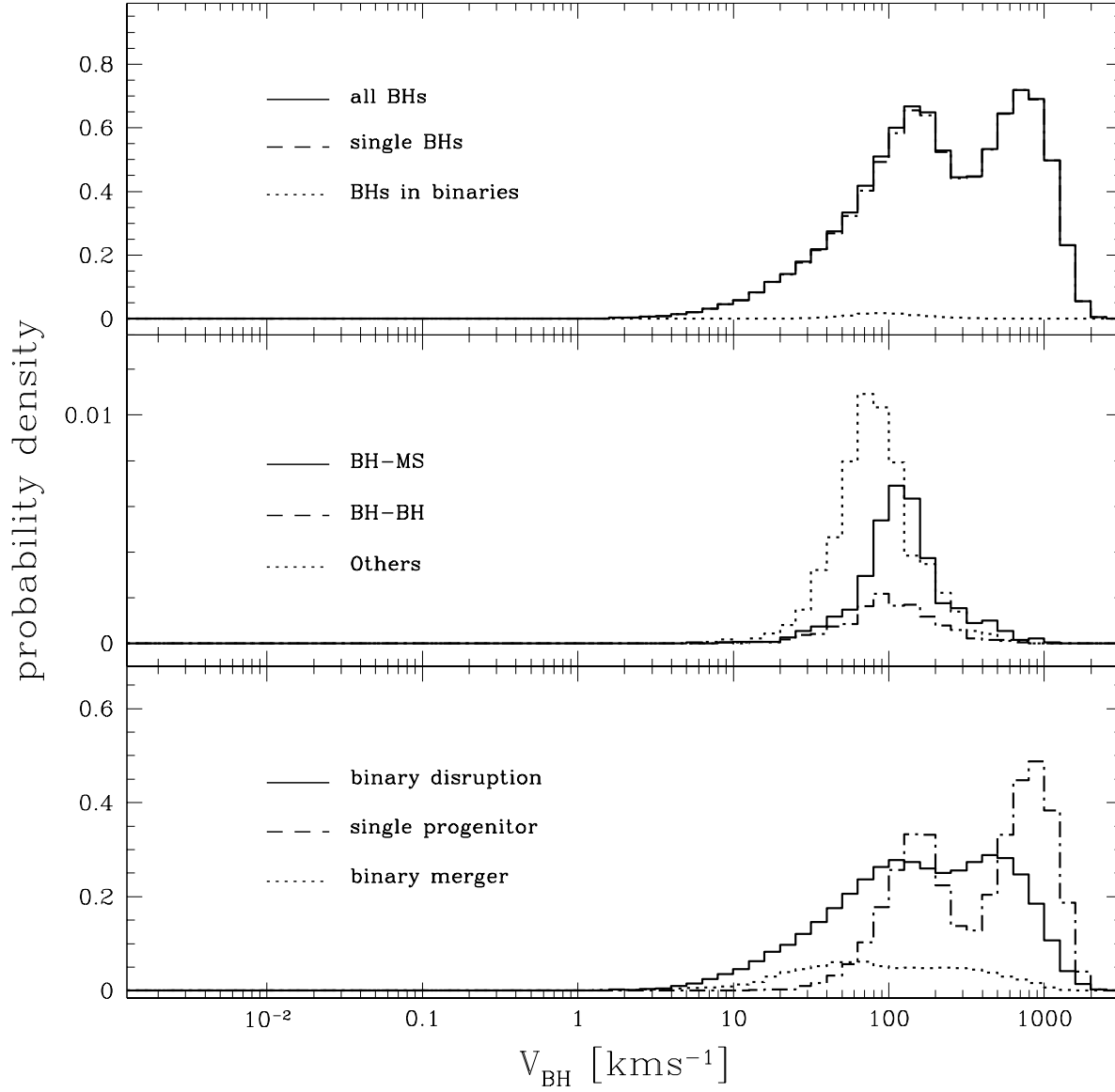


FIG. 16.— Spatial velocities of black holes at $t = 103.8 \text{ Myr}$ after the starburst for Model E. Lines same as for Fig. 2. Note absence of the no-kick BHs (cf. Fig. 2).

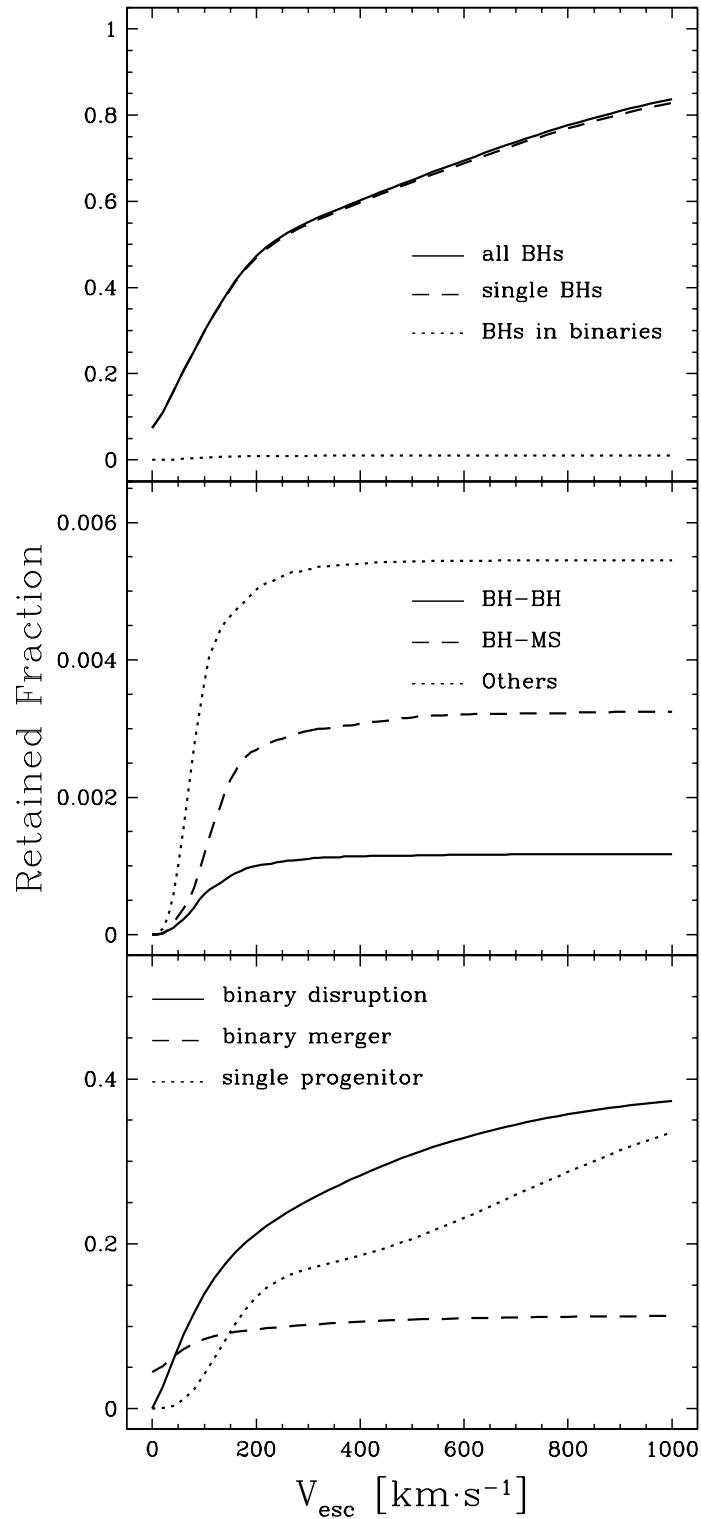


FIG. 17.— Retained fraction (cluster population) of BHs as a function of V_{esc} for model E and $t = 103.8$ Myr. Line styles are the same as for Fig. 4. All curves are normalized to the total number of BHs (single and binaries) formed in the standard model simulation. Note that the fraction showing all BHs does not reach unity, since there is still a small number of BHs with velocities over 1000 km s^{-1} .